Mon. Not. R. Astron. Soc. **345,** 325–339 (2003)

Compressible magnetohydrodynamic turbulence: mode coupling, scaling relations, anisotropy, viscosity-damped regime and astrophysical implications

Jungyeon Cho[1⋆] and A. Lazarian[2⋆]
Astronomy Department, University of Wisconsin-Madison, 475 N. Charter St., Madison, WI 53706, USA

Accepted 2003 June 24. Received 2003 June 19; in original form 2003 January 20

ABSTRACT

We present numerical simulations and explore scalings and anisotropy of compressible magnetohydrodynamic (MHD) turbulence. Our study covers both gas-pressure-dominated (high β) and magnetic-pressure-dominated (low β) plasmas at different Mach numbers. In addition, we present results for super-Alfvénic turbulence and discuss in what way it is similar to sub-Alfvénic turbulence. We describe a technique of separating different magnetohydrodynamic modes (slow, fast and Alfvén) and apply it to our simulations. We show that, for both high- and low-β cases, Alfvén and slow modes reveal a Kolmogorov $k^{-5/3}$ spectrum and scale-dependent Goldreich–Sridhar anisotropy, while fast modes exhibit a $k^{-3/2}$ spectrum and isotropy. We discuss the statistics of density fluctuations arising from MHD turbulence in different regimes. Our findings entail numerous astrophysical implications ranging from cosmic ray propagation to gamma ray bursts and star formation. In particular, we show that the rapid decay of turbulence reported by earlier researchers is not related to compressibility and mode coupling in MHD turbulence. In addition, we show that magnetic field enhancements and density enhancements are marginally correlated. Addressing the density structure of partially ionized interstellar gas on astronomical-unit scales, we show that the viscosity-damped regime of MHD turbulence that we reported earlier for incompressible flows persists for compressible turbulence and therefore may provide an explanation for these mysterious structures.

Key words: MHD – turbulence – ISM: general.

1 INTRODUCTION

Astrophysical turbulence is ubiquitous and it holds the key to many astrophysical processes (star formation, heating of the interstellar medium, properties of accretion discs, cosmic ray transport, etc.). Therefore understanding of turbulence is a necessary requirement for making further progress in any of these directions. Unlike laboratory turbulence, astrophysical turbulence is magnetized and highly compressible.

Turbulence has been studied in the context of the interstellar medium (ISM) and the solar wind. The ISM in the Milky Way and neighbouring galaxies is known to be turbulent on scales ranging from astronomical units (AUs) to kiloparsecs (Armstrong, Rickett & Spangler 1995; Deshpande, Dwarakanath & Goss 2000; Stanimirovic & Lazarian 2001). The solar wind also exhibits small-scale turbulence (Leamon et al. 1998). The measured statistics of fluctuations in the ISM and the solar wind is consistent with the Kolmogorov turbulence obtained for an incompressible unmagnetized fluid. This surprising observational evidence[1] resulted in numerous attempts to use Kolmogorov statistics for practical computations of astrophysical quantities, e.g. cosmic ray scattering. We shall show below that in most cases such calculations bring *erroneous* results.

Why would we expect astrophysical fluids to be turbulent and how can we study astrophysical turbulence? A fluid of viscosity ν becomes turbulent when the rate of viscous dissipation, which is $\sim\nu/L^2$ at the energy injection scale L, is much smaller than the energy transfer rate $\sim V_L/L$, where V_L is the velocity dispersion at the scale L. The ratio of the two rates is the Reynolds number $Re = V_L L/\nu$. In general, when Re is larger than 10–100 the system

⋆E-mail: cho@astro.wisc.edu (JC); lazarian@astro.wisc.edu (AL)

[1] The ambiguities of data interpretation were frequently quoted to justify ignoring this fact. For instance, electron density fluctuations discussed in Armstrong et al. (1995) provide only indirect evidence for a Kolmogorov-type spectrum. However, the solar wind observations are made *in situ* and are more difficult to disregard. Moreover, a newly developed statistical technique (Lazarian & Pogosyan 2000) allowed us to measure the Kolmogorov-type spectrum of velocity fluctuations (see also Lazarian & Esquivel 2003).

becomes turbulent. Chaotic structures develop gradually as Re increases, and those with $Re \sim 10^3$ are appreciably less chaotic than those with $Re \sim 10^8$. Observed features such as star-forming clouds are very chaotic for $Re > 10^8$. This not only ensures that the fluids are turbulent but also makes it difficult to simulate the turbulence. The currently available 3D simulations for 512 cubes can have Re up to $\sim O(10^3)$ and are limited by their grid sizes. Therefore, it is essential to find 'scaling laws' in order to extrapolate numerical calculations ($Re \sim O(10^3)$) to real astrophysical fluids ($Re > 10^8$). We show below that even with its limited resolution, numerics is a great tool for testing scaling laws.

Kolmogorov theory provides a scaling law for incompressible non-magnetized hydrodynamic turbulence (Kolmogorov 1941). This law is true in the statistical sense and it provides a relation between the relative velocity v_l of fluid elements and their separation l, namely, $v_l \sim l^{1/3}$. An equivalent description is to express the spectrum $E(k)$ as a function of wavenumber k ($\sim 1/l$). The two descriptions are related by $kE(k) \sim v_l^2$. The famous Kolmogorov spectrum is $E(k) \sim k^{-5/3}$. The applications of Kolmogorov theory range from engineering research to meteorology (see Monin & Yaglom 1975) but its astrophysical applications are poorly justified.

Let us consider incompressible magnetohydrodynamic (MHD) turbulence first. It has long been understood that MHD turbulence is anisotropic[2] (e.g. Shebalin, Matthaeus & Montgomery 1983). Substantial progress has been achieved recently by Goldreich & Sridhar (1995, hereafter GS95) who made an ingenious prediction regarding relative motions parallel and perpendicular to the magnetic field $\boldsymbol{B}$ for incompressible MHD turbulence. The GS95 model envisages a Kolmogorov spectrum of velocity and scale-dependent anisotropy (see below). These relations have been confirmed numerically (Cho & Vishniac 2000b; Maron & Goldreich 2001; Cho, Lazarian & Vishniac 2002a, hereafter CLV02a; see also CLV03a) and are in good agreement with observed and inferred astrophysical spectra (see CLV03a). A remarkable fact revealed in CLV02a is that fluid motions perpendicular to $\boldsymbol{B}$ are identical to hydrodynamic motions. This provides an essential physical insight into why in some respects MHD turbulence and hydrodynamic turbulence are similar, while in other respects they are different.

The GS95 model considered incompressible MHD, but the real ISM is highly compressible. The literature on the properties of compressible MHD is very rich (see CLV03a). Back in the 1980s Higdon (1984) theoretically studied density fluctuations in interstellar MHD turbulence. Matthaeus & Brown (1988) studied nearly incompressible MHD at low Mach number and Zank & Matthaeus (1993) extended it. In an important paper Matthaeus et al. (1996) numerically explored the anisotropy of compressible MHD turbulence. However, those papers do not provide universal scalings of the GS95 type.

Is it feasible to obtain scaling relations for compressible MHD turbulence? Some hints about the effects of compressibility can be inferred from the seminal paper of Goldreich & Sridhar (GS95). A more focused discussion was presented in the paper by Lithwick & Goldreich (2001) which deals with electron density fluctuations in a gas-pressure-dominated plasma, i.e. in the high-β regime ($\beta \equiv P_{\rm gas}/P_{\rm mag} \gg 1$). The incompressible regime formally corresponds to $\beta \to \infty$ and therefore it is natural to expect that for $\beta \gg 1$ the GS95 picture would persist. Lithwick & Goldreich (2001) also speculated that for low-β plasmas the GS95 scaling of slow modes may be applicable. An important study of MHD modes in compressible low-β plasmas is given in Cho & Lazarian (2002a; hereafter CL02) where we developed and tested our technique of separating different MHD modes.

In this work, we provide a detailed study of mode coupling and scalings of compressible (fast and slow) and Alfvénic modes in high-β, intermediate, and low-β plasmas. Our approach is complementary to that employed in direct numerical simulations of astrophysical turbulence. In such simulations, e.g. in those dealing with the interstellar medium (see Vazquez-Semadeni et al. 2000b), simulations of particular astrophysical objects, e.g. molecular clouds, are attempted. These simulations provide synthetic maps that can be compared with observations. Our goal is to obtain scaling laws that can also be compared with observations. In Section 2, we describe our approach to the problem including both simple theoretical considerations and expectations that motivate our study, and the numerical technique that we employ. In Section 3, we present velocity spectra and anisotropies for high- and low-β plasmas. In Section 4, we discuss scalings of density and magnetic field. In Section 5, we present a study of the viscosity-damped regime of MHD turbulence in a compressible fluid. This study extends our earlier work (Cho, Lazarian & Vishniac 2002b, henceforth CLV02b) where this regime was reported for incompressible flows. In Section 6, we discuss the astrophysical implications of our results, including the rate of MHD turbulence decay, the relation between the decay rate and compressibility, the correlation of density and magnetic field, and the formation of density structures at the AU scale. The summary is given in Section 7.

2 OUR APPROACH

2.1 Theoretical considerations

Let us start with a discussion of why isotropic Kolmogorov turbulence cannot be applicable for describing strongly magnetized gas. Assume that, at some large-scale L, the magnetic energy and kinetic energy are equal: $\rho V_L^2/2 \sim B^2/(8\pi)$. According to the Kolmogorov theory, the kinetic energy at scale $l < L$ is $\rho V_l^2/2 \sim (l/L)^{2/3}(\rho V_L^2/2)$, which is smaller than the large-scale kinetic energy by a factor of $(l/L)^{2/3}$. But, the magnetic energy density does not diminish as the scale reduces. Therefore, at scales smaller than L, hydrodynamic motions will not be able to bend magnetic field lines substantially.

An important observation that leads to understanding of the GS95 scaling is that the magnetic field cannot prevent mixing motions of magnetic field lines if the motions are perpendicular to the magnetic field. These motions will, however, cause waves that will propagate along magnetic field lines. If that is the case, the time-scale of the wave-like motions, i.e. $\sim l_\parallel/V_{\rm A}$, where $l_\parallel$ is the characteristic size of the perturbation along the magnetic field and $V_{\rm A} = B/\sqrt{4\pi\rho}$ is the local Alfvén speed, will be equal to the hydrodynamic time-scale, $l_\perp/v_l$, where $l_\perp$ is the characteristic size of the perturbation perpendicular to the magnetic field. The mixing motions are hydrodynamic-like[3] and therefore obey Kolmogorov scaling $v_l \propto l_\perp^{1/3}$. Combining the two relations above we can get the GS95 anisotropy, $l_\parallel \propto l_\perp^{2/3}$

[2] It is not possible to cite all the important papers in the area of MHD turbulence. An incomplete list of the references in a recent review on the statistics of MHD turbulence by Cho, Lazarian & Vishniac (2003a, henceforth CLV03a) includes about 200 entries.

[3] Recent simulations (Cho et al. 2003b) suggest that perpendicular mixing is indeed efficient for mean magnetic fields of up to the equipartition value. This corresponds to our earlier result that high-order velocity statistics of MHD turbulence in the perpendicular directions is very similar to that of hydrodynamic turbulence (CLV02a).

(or $k_\parallel \propto k_\perp^{2/3}$ in terms of wavenumbers). If we interpret $l_\parallel$ as the eddy size in the direction of the local[4] magnetic field and $l_\perp$ as that in the perpendicular directions, the relation implies that smaller eddies are more elongated (see Appendix B for an illustration of scale-dependent anisotropy).

How is this idealized incompressible model related to the actual, e.g. interstellar, turbulence? Compressible MHD turbulence is a highly non-linear phenomenon and it has been thought that different types of perturbations or modes (Alfvén, slow and fast) in compressible media are strongly coupled. Nevertheless, one may question whether this is true. A remarkable feature of the GS95 model is that Alfvén perturbations cascade to small scales over just one wave period, while the other non-linear interactions require more time. Therefore one might expect that the non-linear interactions with other types of waves should affect the Alfvénic cascade only marginally. Moreover, as the Alfvén waves are incompressible, the properties of the corresponding cascade may not depend on the sonic Mach number.

The generation of compressible motions (i.e. radial components in Fourier space) from Alfvénic turbulence is a measure of mode coupling. How much energy in compressible motions is drained from the Alfvénic cascade? According to the closure calculations (Bertoglio, Bataille & Marion 2001; see also Zank & Matthaeus 1993), the energy in compressible modes in hydrodynamic turbulence scales as $\sim M_{\rm s}^2$ if $M_{\rm s} < 1$. We may conjecture that this relation can be extended to MHD turbulence if, instead of $M_{\rm s}^2$, we use $\sim(\delta V)^2{}_{\rm A}/(a^2 + V_{\rm A}^2)$. (Hereinafter, we define $V_{\rm A} \equiv B_0/\sqrt{4\pi\rho}$, where B_0 is the mean magnetic field strength.) However, as the Alfvén modes are anisotropic, this formula may require an additional factor. The compressible modes are generated inside the so-called Goldreich–Sridhar cone, which takes up $\sim(\delta V)_{\rm A}/V_{\rm A}$ of the wavevector space. The ratio of compressible to Alfvénic energy inside this cone is the ratio given above. If the generated fast modes become isotropic (see below), the diffusion or, 'isotropization' of the fast wave energy in the wavevector space increases their energy by a factor of $\sim V_{\rm A}/(\delta V)_{\rm A}$. This results in

$$\frac{(\delta V)^2_{\rm rad}}{(\delta V)^2_{\rm A}} \lesssim \left[\frac{V_{\rm A}^2 + a^2}{(\delta V)^2_{\rm A}}\frac{(\delta V)_{\rm A}}{V_{\rm A}}\right]^{-1}, \qquad (1)$$

where $(\delta V)^2{}_{\rm rad}$ and $(\delta V)^2_{\rm A}$ are the energies of the compressible[5] and Alfvén modes, respectively. Equation (1) suggests that the drain of energy from the Alfvénic cascade is marginal when the amplitudes of perturbations are weak, i.e. $(\delta V)_{\rm A} \ll V_{\rm A}$.

If the Alfvén cascade evolves on its own, it is natural to assume that slow modes exhibit GS95 scaling. Indeed, slow modes in gas-pressure-dominated environments (high-β plasmas) are similar to the pseudo-Alfvén modes in the incompressible regime (see GS95; Lithwick & Goldreich 2001). The latter modes do follow the GS95 scaling. In magnetic-pressure-dominated environments (low-β plasmas), slow modes are density perturbations propagating with the sound speed a parallel to the mean magnetic field (see equation A31). These perturbations are essentially static for $a \ll V_{\rm A}$. Therefore Alfvénic turbulence is expected to mix density perturbations as if they were passive scalar. This also induces the GS95 spectrum.

[4] The concept of local is crucial. The GS95 scalings are obtained only in the local frame of the magnetic field, as this is the frame where magnetic fields are allowed to be mixed without being opposed by magnetic tension.

[5] It is possible to show that the compressible modes inside the Goldreich–Sridhar cone are basically fast modes.

The fast waves in the low-β regime propagate at $V_{\rm A}$ irrespective of the magnetic field direction. In the high-β regime, the properties of fast modes are similar, but the propagation speed is the sound speed a. Thus the mixing motions induced by Alfvén waves should marginally affect the fast wave cascade. This is expected to be analogous to the acoustic wave cascade and hence isotropic.

For most part of this paper, we shall assume that $\delta V \sim \delta B/\sqrt{4\pi\rho} \sim B_0/\sqrt{4\pi\rho}$, where δB is the rms strength of the random magnetic field. This is less restrictive than it might appear, since as long as there is some scale l' in the turbulent cascade where $v_{l'} \sim B/\sqrt{4\pi\rho}$ we can take $L = l'$, $V_L = v_{l'}$ and use this model of turbulence for all smaller scales. Suppose that we have a turbulent system initially threaded by a mean magnetic field only. If initially the turbulent energy is larger than the magnetic energy of the mean field, we are in the regime of so-called super-Alfvénic turbulence. In this regime the growth of the magnetic field is expected through the so-called 'turbulent dynamo' (see Batchelor 1950; Brandenburg et al. 1996; Cho & Vishniac 2000a). Initially, the growth of magnetic energy is most active at a scale roughly an order of magnitude larger than the dissipation scale and the magnetic spectrum peaks at the scale where the growth of magnetic energy is most active. As the magnetic energy grows, the magnetic back-reaction becomes important at the initially most active scale and the peak of the magnetic power spectrum moves to larger scales. Finally, when equipartition between the kinetic and magnetic energy densities occurs at a scale somewhat (factor of 2 or 3) smaller than the kinetic energy peak, turbulence reaches a statistically stationary state. This agrees well with the results of incompressible simulations in Cho & Vishniac (2000a). However, this is not a universally accepted idea. For example, Padoan & Nordlund (1999) reported that, in their compressible simulations, the power spectrum of $\rho^{1/2}v$ has a shallower slope then those of the velocity and magnetic field, which implies that equipartition between kinetic magnetic energy cannot be reached at small scales. At scales smaller than the equipartition scale, the turbulence becomes sub-Alfvénic and our earlier considerations should be applicable.

The arguments above suggest that compressible MHD turbulence should demonstrate well-defined scaling relations. Below we test these arguments and reveal scaling relations for different βs and Mach numbers.

2.2 Numerical scheme

We use a third-order accurate hybrid, essentially non-oscillatory (ENO) scheme (see CL02) to solve the ideal isothermal MHD equations in a periodic box:

$$\partial\rho/\partial t + \nabla\cdot(\rho\mathbf{v}) = 0, \qquad (2)$$

$$\partial\boldsymbol{v}/\partial t + \boldsymbol{v}\cdot\nabla\boldsymbol{v} + \rho^{-1}\nabla(a^2\rho) - (\nabla\times\boldsymbol{B})\times\boldsymbol{B}/4\pi\rho = \boldsymbol{f}, \qquad (3)$$

$$\partial\boldsymbol{B}/\partial t - \nabla\times(\boldsymbol{v}\times\boldsymbol{B}) = 0, \qquad (4)$$

with $\nabla\cdot\boldsymbol{B} = 0$ and an isothermal equation of state. Here $\boldsymbol{f}$ is a random large-scale driving force, ρ is the density, $\boldsymbol{v}$ is the velocity, and $\boldsymbol{B}$ is the magnetic field. The rms velocity δV is maintained to be approximately unity (in fact $\delta V \sim 0.7$), so that $\boldsymbol{v}$ can be viewed as the velocity measured in units of the rms velocity of the system and $\boldsymbol{B}/\sqrt{4\pi\rho}$ as the Alfvén velocity in the same units. The time t is in units of the large eddy turn-over time ($\sim L/\delta V$) and the length in units of L, the scale of the energy injection. The magnetic field consists of the uniform background field and a fluctuating field: $\boldsymbol{B} = \boldsymbol{B}_0 + \boldsymbol{b}$.

For mode coupling studies (Section 3.1), we do not drive turbulence. For scaling studies, we drive turbulence solenoidally in

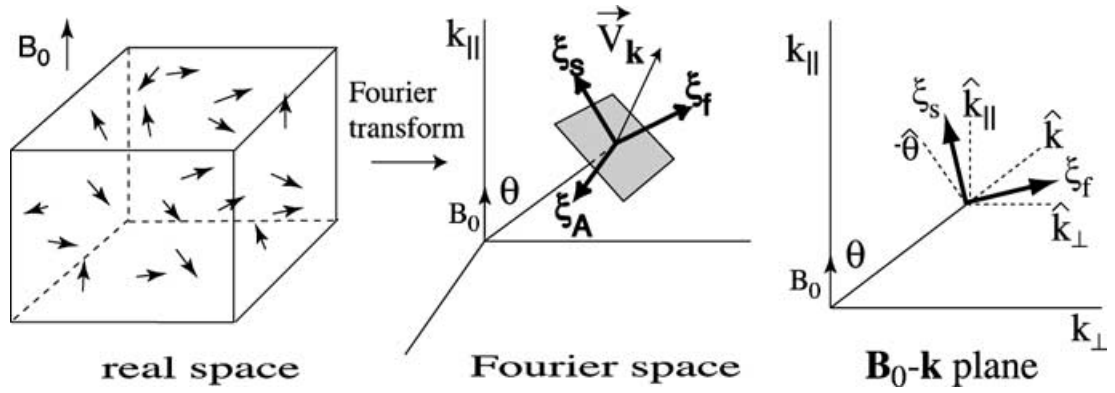

Figure 1. Separation method. We separate Alfvén, slow, and fast modes in the Fourier space by projecting the velocity Fourier component $\boldsymbol{v_k}$ on to bases $\boldsymbol{\xi}_{\rm A}$, $\boldsymbol{\xi}_{\rm s}$, and $\boldsymbol{\xi}_{\rm f}$, respectively. Note that $\boldsymbol{\xi}_{\rm A} = -\hat{\boldsymbol{\varphi}}$. The slow basis $\boldsymbol{\xi}_{\rm s}$ and fast basis $\boldsymbol{\xi}_{\rm f}$ lie in the plane defined by $\boldsymbol{B}_0$ and $\boldsymbol{k}$. The slow basis $\boldsymbol{\xi}_{\rm s}$ lies between $-\hat{\boldsymbol{\theta}}$ and $\hat{\boldsymbol{k}}_{\|}$. The fast basis $\boldsymbol{\xi}_{\rm f}$ lies between $\hat{\boldsymbol{k}}$ and $\hat{\boldsymbol{k}}_{\perp}$.

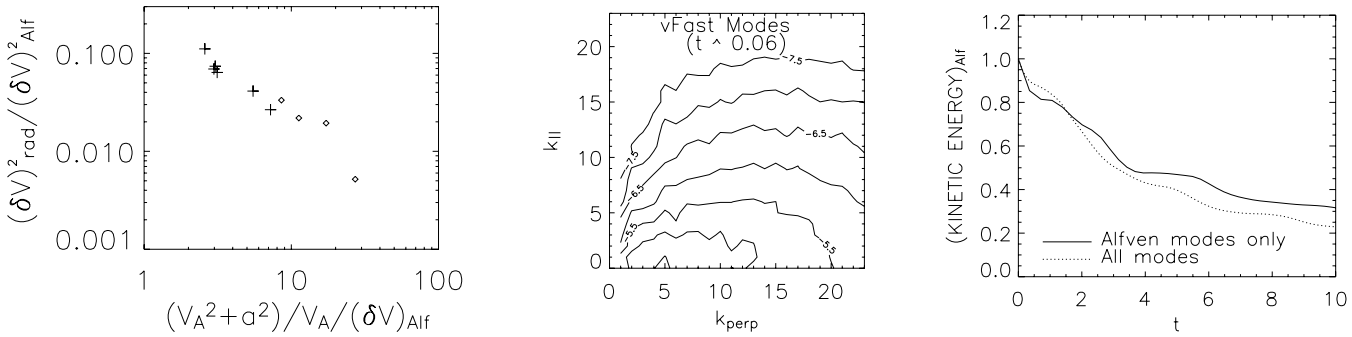

Figure 2. Mode coupling studies. (a) Left: square of the rms velocity of the compressible modes. We use 144^3 grid points. Only Alfvén modes are allowed as the initial condition. 'Pluses' are for low-β cases ($0.02 \leqslant \beta \leqslant 0.4$). 'Diamonds' are for high-β cases ($1 \leqslant \beta \leqslant 20$). (b) Middle: generation of fast modes. Snapshot is taken at $t = 0.06$ from a simulation (with 144^3 grid points) that started off with Alfvén modes only. Initially, β (the ratio of gas to magnetic pressure, $P_g/P_{\rm mag}$) is 0.2 and $M_{\rm s}$ (the sonic Mach number) is ∼1.6. (c) Right: comparison of decay rates. The decay of Alfvén modes is not much affected by other (slow and fast) modes. We use 216^3 grid points. Initially, $\beta = 0.02$ and $M_{\rm s} \sim 4.5$ for the solid line and $M_{\rm s} \sim 7$ for the dotted line. Note that initial data are, in some sense, identical for the solid and the dotted lines. The sonic Mach number for the solid line is smaller because we removed fast and slow modes from the initial data before the decay simulation. For the dotted line, we did not remove any modes from the initial data.

Fourier space and use 216^3 points, $V_{\rm A} = B_0/\sqrt{4\pi\rho} = 1$, and $\rho_0 = 1$. The average rms velocity in the statistically stationary state is $\delta V \sim 0.7$.

For our calculations we assume that $B_0/\sqrt{4\pi\rho} \sim \delta B/\sqrt{4\pi\rho} \sim \delta V$. In this case, the sound speed is the controlling parameter and basically two regimes can exist: supersonic and subsonic. Note that supersonic means low β and subsonic means high β. When supersonic, we consider mildly supersonic (or, mildly low β) and highly supersonic (or, very low β).[6]

2.3 Separation of MHD modes

Three types of waves exist (Alfvén, slow and fast) in a compressible magnetized plasma. The slow, fast, and Alfvén bases that denote the direction of displacement vectors for each mode are given by

$$\hat{\boldsymbol{\xi}}_{\rm s} \propto (-1+\alpha-\sqrt{D})k_{\|}\hat{\boldsymbol{k}}_{\|} + (1+\alpha-\sqrt{D})k_{\perp}\hat{\boldsymbol{k}}_{\perp}, \quad (5)$$

$$\hat{\boldsymbol{\xi}}_{\rm f} \propto (-1+\alpha+\sqrt{D})k_{\|}\hat{\boldsymbol{k}}_{\|} + (1+\alpha+\sqrt{D})k_{\perp}\hat{\boldsymbol{k}}_{\perp}, \quad (6)$$

$$\hat{\boldsymbol{\xi}}_{\rm A} = -\hat{\boldsymbol{\varphi}} = \hat{\boldsymbol{k}}_{\perp} \times \hat{\boldsymbol{k}}_{\|}, \quad (7)$$

where $D = (1+\alpha)^2 - 4\alpha\cos\theta$, $\alpha = a^2/V_{\rm A}^2 = \beta(\gamma/2)$, θ is the angle between $\boldsymbol{k}$ and $\boldsymbol{B}_0$, and $\hat{\boldsymbol{\varphi}}$ is the azimuthal basis in the spherical polar coordinate system. These are equivalent to the expression in CL02:

$$\hat{\boldsymbol{\xi}}_{\rm s} \propto k_{\|}\hat{\boldsymbol{k}}_{\|} + \frac{1-\sqrt{D}-\beta/2}{1+\sqrt{D}+\beta/2}\left[\frac{k_{\|}}{k_{\perp}}\right]^2 k_{\perp}\hat{\boldsymbol{k}}_{\perp}, \quad (8)$$

$$\hat{\boldsymbol{\xi}}_{\rm f} \propto \frac{1-\sqrt{D}+\beta/2}{1+\sqrt{D}-\beta/2}\left[\frac{k_{\perp}}{k_{\|}}\right]^2 k_{\|}\hat{\boldsymbol{k}}_{\|} + k_{\perp}\hat{\boldsymbol{k}}_{\perp}. \quad (9)$$

(Note that $\gamma = 1$ for the isothermal case.)

The slow and fast velocity components can be obtained by projecting the velocity Fourier component $\boldsymbol{v_k}$ on to $\hat{\boldsymbol{\xi}}_{\rm s}$ and $\hat{\boldsymbol{\xi}}_{\rm f}$, respectively (Fig. 1). In Appendix A, we discuss how to separate the slow and fast magnetic modes. We obtain energy spectra using this projection method. When we calculate the structure functions (e.g. for the Alfvén velocity) in real space, we first obtain the Fourier components using the projection and then we obtain the real space values by performing a Fourier transform.

[6] The terms 'mildly' and 'highly' are somewhat arbitrary terms. We consider these two supersonic cases to cover a broad range of parameter space. Note that Boldyrev, Nordlund & Padoan (2002b) recently provided a Mach number dependence study of the compressible MHD turbulence statistics where only two regimes are manifest: essentially incompressible and essentially compressible shock dominated (with smooth transition at some $M_{\rm s}$ of order unity).

3 VELOCITY SCALINGS

3.1 Mode coupling

In CL02 we demonstrated the decoupling of Alfvén and fast modes in low-β plasmas. Here we substantially extend the CL02 analysis. As mentioned above, the coupling of compressible and incompressible modes is crucial. If Alfvénic modes produce a copious number of compressible modes, the whole picture of independent Alfvénic turbulence fails. However, our calculations show that the amount of energy drained into compressible motions is negligible, provided that either the external magnetic field or the gas pressure is sufficiently high. Fig. 2(a) suggests that the generation of compressible motions follows equation (1). Fast modes also follow a similar scaling, although the scatter is a bit larger. The marginal generation of compressible modes is in agreement with earlier studies by Boldyrev et al. (2002b) and Porter, Pouquet & Woodward (2002), where the velocity was decomposed into a potential component and a solenoidal component. See Fig. 2(a) for the values of $\sim\chi$ (= the ratio of the mean square potential to solenoidal velocity). Fig. 2(b) demonstrates that fast modes are initially generated anisotropically, which supports our theoretical consideration in Section 2.1.

Fig. 2(c) shows that the dynamics of Alfvén modes is not affected by slow modes. We first perform a driven turbulence simulation with 216^3 grid point, $\beta \sim 0.02$, and $M_s \sim 7$. Then, after it has reached a statistically stationary state, we stop the run and save the data. Using these data, we perform two decay simulations. For one (the solid line), we remove all slow and fast modes and let the turbulence decay. For the other (the dotted line), without removing any modes, we just let the turbulence decay. The solid line in the figure is the energy in Alfvén modes when we start the decay simulation with Alfvén modes only. The dotted line is the Alfvén energy when we start the simulation with all modes. This result confirms that the cascade of Alfvén modes is almost independent of the slow and fast modes. In this sense, coupling between Alfvén and other modes is weak.

3.2 High-β and mildly supersonic low-β regimes

Alfvén modes. Fig. 3(a) (low-β) and Fig. 4(a) (high-β) show that the power spectra of Alfvén waves follow a Kolmogorov spectrum:

$$\text{Spectrum of Alfvén waves:} \quad E^A(k) \propto k_\perp^{-5/3}. \tag{10}$$

In Fig. 3(b) (middle-left panel) and Fig. 4(b) (middle-left panel), we plot contours of equal second-order structure function for the velocity ($\mathrm{SF}_2(\boldsymbol{r}) = \langle |\, \boldsymbol{v}\,(\boldsymbol{x}+\boldsymbol{r}) - \boldsymbol{v}(\boldsymbol{x})|^2 \rangle_{\mathrm{avg.over}\boldsymbol{x}}$) obtained in local coordinate systems in which the parallel axis is aligned with the local mean field (see Cho & Vishniac 2000b; Maron & Goldreich 2001; CLV02a). The SF_2 along the axis perpendicular to the local

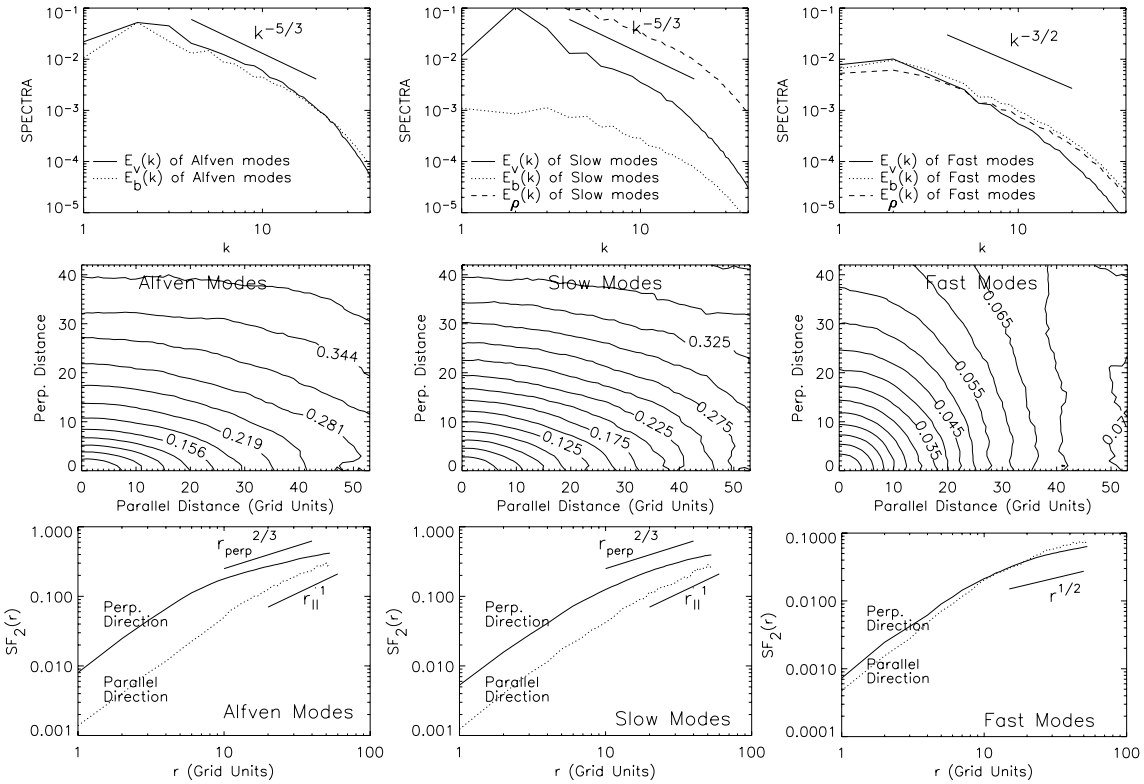

Figure 3. Low β ($\beta \sim 0.2$ and $M_s \sim 2.3$) scaling relations. Results from driven turbulence with M_A (the Alfvén Mach number) $\sim$0.7, and 216^3 grid points. ($V_A \equiv B_0/\sqrt{4\pi\rho} = 1$; sound speed $a = \sqrt{0.1}$; $\delta V \sim 0.7$.) (a) Upper-left: spectra of Alfvén modes follow a Kolmogorov-like power law. (b) Middle-left: the second-order structure function (SF_2) for the velocity of Alfvén modes shows anisotropy similar to GS95 ($r_\parallel \propto r_\perp^{2/3}$ or $k_\parallel \propto k_\perp^{2/3}$). The structure functions are measured in directions perpendicular or parallel to the local mean magnetic field in real space. We obtain the real-space velocity and magnetic fields by inverse Fourier transform of the projected fields. (c) Lower-left: SF_2 on the parallel axis and on the perpendicular axis for Alfvén-mode velocity. (d) Upper-middle: spectra of slow modes also follow a Kolmogorov-like power law. (e) Middle-middle: slow-mode velocity shows anisotropy similar to GS95. (f) Lower-middle: SF_2 on the parallel axis and on the perpendicular axis for slow-mode velocity. (g) Upper-right: spectra of fast modes are compatible with the Iroshnikov–Kraichnan spectrum. (h) Upper-middle: the SF_2 of the fast-mode velocity shows isotropy. The fast-mode magnetic field also shows isotropy. (i) Lower-right: SF_2 on the parallel axis and on the perpendicular axis for fast-mode velocity.

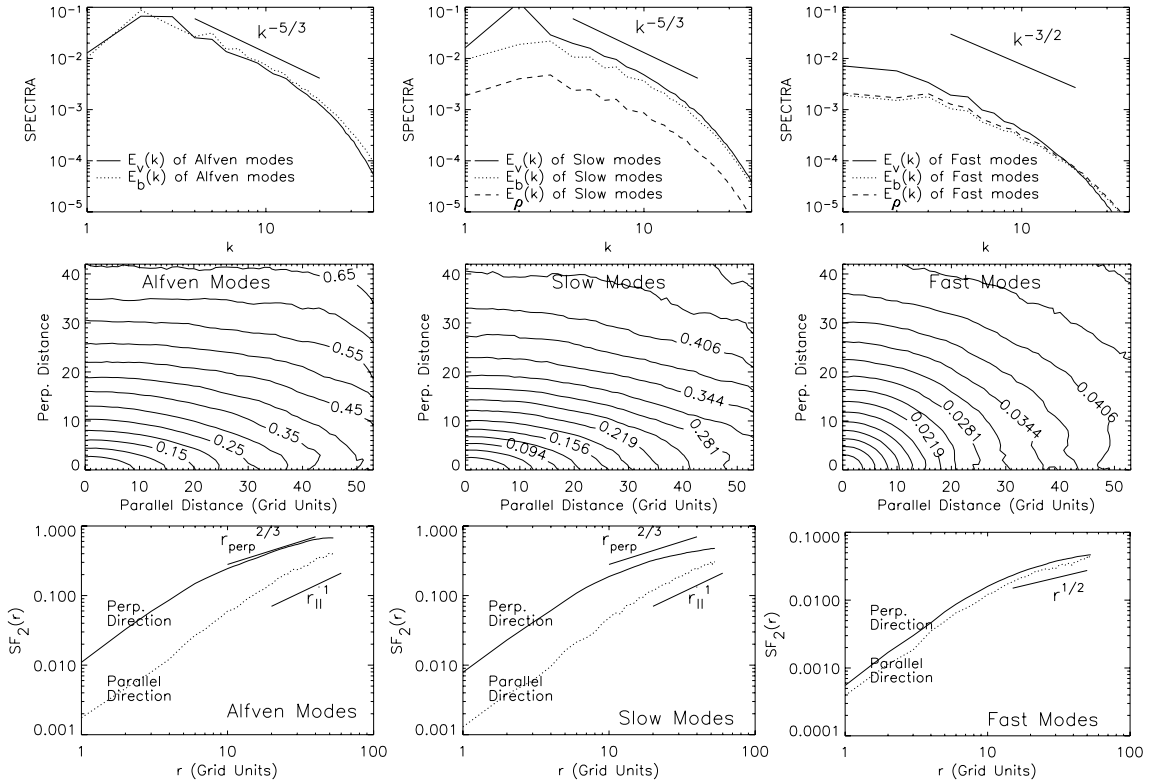

Figure 4. High β ($\beta \sim 4$ and $M_s \sim 0.35$). $V_A \equiv B_0/\sqrt{4\pi\rho} = 1$, sound speed $a = \sqrt{2}$, $\delta V \sim 0.7$. See the caption in Fig. 3. Alfvén and slow modes follow the GS95 scalings. Fast modes are isotropic.

mean magnetic field follows a scaling compatible with $r^{2/3}$. The SF_2 along the axis parallel to the local mean field follows steeper r^1 scaling (Figs 3c and 4c: lower-left panels). The results show reasonable agreement with the GS95 model for incompressible MHD turbulence:

$$\text{Anisotropy of Alfvén waves:} \quad r_\parallel \propto r_\perp^{2/3}, \text{ or } k_\parallel \propto k_\perp^{2/3}, \tag{11}$$

where $r_\parallel$ and $r_\perp$ are the semimajor axis and semiminor axis of eddies, respectively (Cho & Vishniac 2000b).

Slow waves. The incompressible limit of slow waves is pseudo-Alfvén waves. Goldreich & Sridhar (1997) argued that the pseudo-Alfvén waves are slaved to the shear-Alfvén (i.e. ordinary Alfvén) waves, which means that pseudo-Alfvén modes do not cascade energy on their own. Lithwick & Goldreich (2001) made similar theoretical arguments for high-β plasmas and conjectured similar behaviour of slow modes in low-β plasmas. We confirmed that similar arguments are also applicable to slow waves in low-β plasmas (CL02). Indeed, the power spectra in Figs 3(d) and 4(d) (upper-middle panels) are consistent with:

$$\text{Spectrum of slow modes:} \quad E^s(k) \propto k_\perp^{-5/3}. \tag{12}$$

In Figs 3(e) and 4(e) (middle-middle panels), contours of equal second-order velocity structure functions (SF_2), representing eddy shapes, show scale-dependent anisotropy: smaller eddies are more elongated. The results show reasonable agreement with GS95-type anisotropy:

$$\text{Anisotropy of slow modes:} \quad k_\parallel \propto k_\perp^{2/3}, \text{ or } r_\parallel \propto r_\perp^{2/3}, \tag{13}$$

where $r_\parallel$ and $r_\perp$ are the semimajor axis and semiminor axis of eddies, respectively.

Fast waves. Figs 3(h) and 4(h) (middle-right panels) show that fast modes are isotropic. The resonance conditions for the interacting fast waves are $\omega_1 + \omega_2 = \omega_3$ and $\boldsymbol{k}_1 + \boldsymbol{k}_2 = \boldsymbol{k}_3$. Since $\omega \propto k$ for the fast modes, the resonance conditions can be met only when all three $\boldsymbol{k}$ vectors are collinear. This means that the direction of the energy cascade is radial in Fourier space. This is very similar to acoustic turbulence, turbulence caused by interacting sound waves (Zakharov 1967; Zakharov & Sagdeev 1970; L'vov, L'vov & Pomyalov 2000). Zakharov & Sagdeev (1970) found $E(k) \propto k^{-3/2}$. However, there is some debate about the exact scaling of acoustic turbulence. Here we cautiously claim that our numerical results are compatible with the Zakharov & Sagdeev scaling:

$$\text{Spectrum of fast modes:} \quad E^f(k) \sim k^{-3/2}. \tag{14}$$

The eddies are isotropic (see also Appendix B).

3.3 Highly supersonic low-β case

The results for low β in the previous subsection are for a Mach number of $\sim$2.3. In this subsection, we present results for a Mach number of $\sim$7. Obviously shock formation is faster when the Mach number of the system is high. We also expect that turbulent motions can compress/disperse the gas more easily when the Mach number is high. As a result, we expect higher density fluctuations when the Mach number is higher. Thus we check the scaling relations for high Mach-number fluids.

Fig. 5 shows that most of the scaling relations that hold true in mildly supersonic flows are still valid in the highly supersonic case. In particular, the anisotropy of Alfvén, slow and fast modes is almost identical to that in the previous section. However, the power

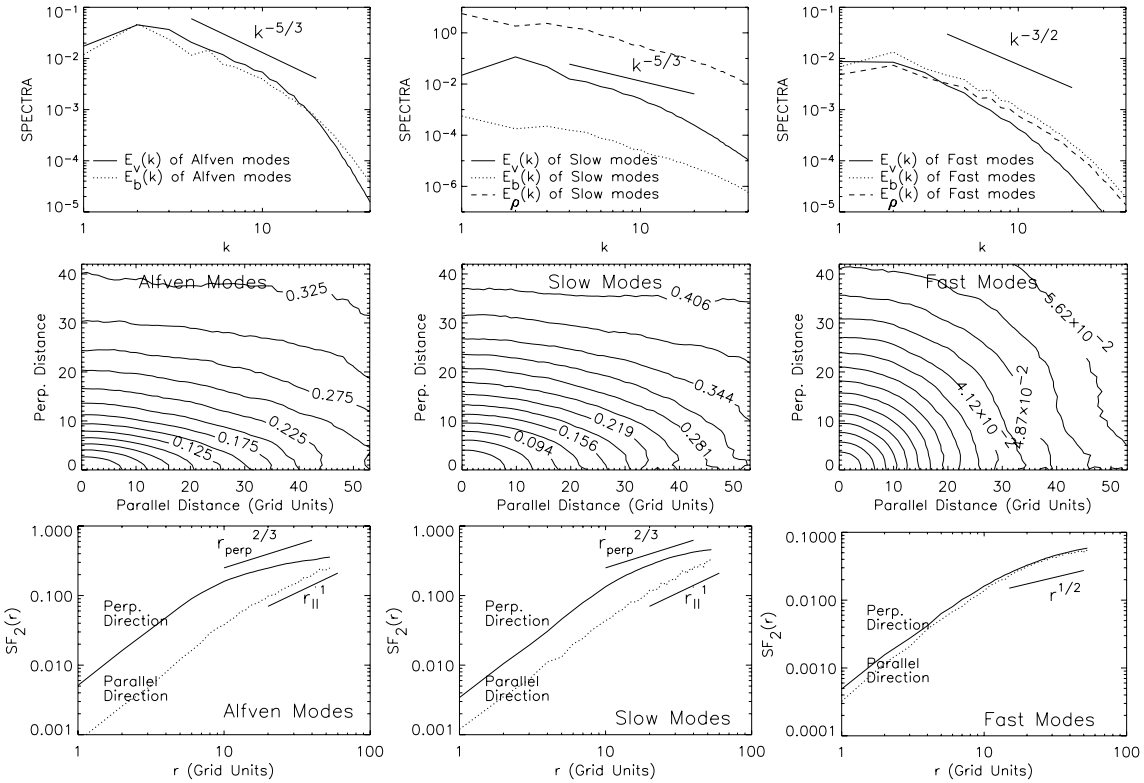

Figure 5. Highly supersonic low β ($\beta \sim 0.02$ and $M_s \sim 7$). $V_A \equiv B_0/\sqrt{4\pi\rho} = 1$, sound speed =0.1, $\delta V \sim 0.7$. Alfvén modes follow the GS95 scalings; slow modes follow the GS95 anisotropy; but the velocity spectrum of slow modes is uncertain. Fast modes are isotropic.

spectra for slow modes do not show the Kolmogorov slope. The slope is close to -2, which is suggestive of shock formation. At this moment, it is not clear whether or not the -2 slope is the true slope. In other words, the observed -2 slope might be due to the limited numerical resolution. Runs with higher numerical resolution should give a definite answer.

3.4 Super-Alfvénic turbulence

So far we have considered sub-Alfvénic turbulence in which the Alfvén speed associated with the mean magnetic field is slightly faster than the rms fluid velocity. If the opposite case is true (i.e. if the mean field B_0 is weak), the turbulence is called super-Alfvénic. In super-Alfvénic turbulence, large-scale magnetic field lines can show very chaotic structures. Whether or not the ISM turbulence is sub-Alfvénic is still a controversial issue.

We mentioned in Section 2.1 that, even in the case of super-Alfvénic turbulence, we can find some scale l' in the turbulent cascade where $v_{l'} \sim B/\sqrt{4\pi\rho}$ and we can apply our model of sub-Alfvénic turbulence for all smaller scales. Fig. 6 supports this idea. The contours in the figure are the second-order structure functions (SF_2) of velocity and magnetic field. We do not use mode decomposition. Nevertheless, the velocity SF_2 reflects scalings of Alfvén and slow modes, because fast modes are weaker than Alfvén and slow modes. As expected, anisotropy emerges at small scales. This is very similar to the incompressible case (Cho & Vishniac 2000a).

Fig. 6(a) shows the power spectra. We notice that the power spectra of the velocity and magnetic field have different shapes. The velocity power spectrum is larger than the magnetic power spectrum near the energy injection scale at $k \sim 2.5$. However, for larger k's ($k > 6$), the magnetic power spectrum is larger than the velocity

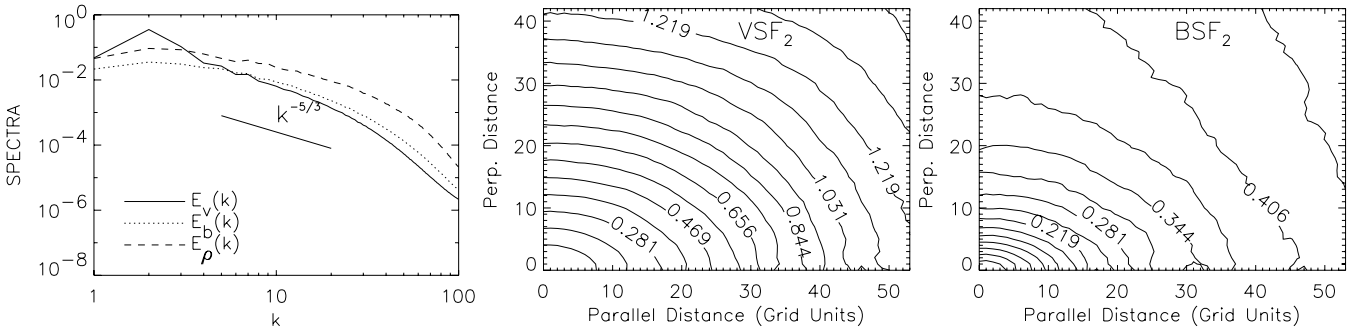

Figure 6. Super-Alfvénic turbulence ($M_A \sim 8$ and $M_s \sim 2.5$). $V_A \equiv B_0/\sqrt{4\pi\rho} = 0.1$, sound speed $a = \sqrt{0.1}$, $\delta V \sim 0.8$. (a) Left: spectra. (b) Middle: the second-order structure function for velocity VSF_2. (c) Right: the second-order structure function for magnetic field BSF_2. No mode decomposition is used for (b) and (c).

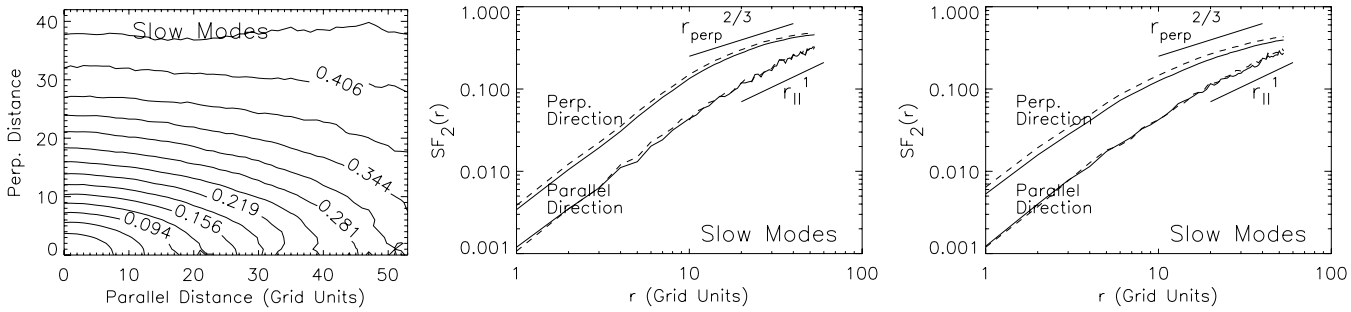

Figure 7. Comparison between the Fourier space method and the real space method. (a) Left: from real space calculation; $M_s \sim 7$. (b) Middle: solid: Fourier space; dashed: real space; $M_s \sim 7$. (c) Right: similar plot for $M_s \sim 2.3$.

spectrum. This behaviour is well known in incompressible simulations with unit magnetic Prandtl number (see, for example, Kida, Yanase & Mizushima 1991; Cho & Vishniac 2000a). Similar behaviour is also observed in earlier compressible simulations (see, for example, Brandenburg et al. 1996). Cho & Vishniac (2000a) argued that the transition from $E_v(k) > E_b(k)$ to $E_v(k) < E_b(k)$ occurs at a wavelength 2 or 3 times larger than that of the energy injection scale.

A careful look at Fig. 6(a) reveals that, for $k < 8$, the power spectrum of velocity declines faster than Kolmogorov as k increases. This is not very surprising because the magnetic field has more power than the velocity at large k's and, therefore, can affect the velocity power spectrum at small k's. Kida et al. (1991) claimed that the sum of $E_v(k) + E_b(k)$ roughly follows the Kolmogorov spectrum in their incompressible simulations. If this is true, then the velocity power spectrum should have a spectrum steeper than Kolmogorov at small k's because many simulations have shown that the magnetic power spectrum is significantly flatter than the velocity spectrum at small k's when the mean field B_0 is weak (Kida et al. 1991; Brandenburg et al. 1996; Cho & Vishniac 2000a). After $k \sim 8$, it seems that the velocity power spectrum gets flatter.

Boldyrev, Nordlund & Padoan (2002a) also obtained a velocity power spectrum steeper than Kolmogorov in their supersonic super-Alfvénic MHD simulations. They attributed the steep spectrum to different intermittency properties compared to the incompressible case. Since they used a different simulation set-up, we do not directly compare our results and theirs. For example, their turbulence is driven at larger scales than ours and their sonic Mach number is larger than ours. Further parameter study is absolutely necessary.

3.5 How good is our technique?

The technique described in Section 2.3 is statistical in nature. That is, we separate each MHD mode with respect to the mean magnetic field $\boldsymbol{B}_0$. This procedure is affected by the wandering of large-scale magnetic field lines, as well as density inhomogeneities.[7]

Nevertheless, we can show that our technique gives statistically correct results. In the low-β regime, the velocity of a slow mode is nearly parallel to the local mean magnetic field. Therefore, for low-β plasmas, we can obtain velocity statistics for slow modes in real space as follows. First, we identify the direction of the local mean magnetic field using the method described in Cho & Vishniac (2000b). Secondly, we calculate the second-order structure function for slow modes by the formula $\mathrm{VSF}_2(\boldsymbol{r}) = \langle |(\boldsymbol{v}(\boldsymbol{x}+\boldsymbol{r}) - \boldsymbol{v}(\boldsymbol{x})) \cdot \hat{\boldsymbol{B}}_l|^2 \rangle$, where $\hat{\boldsymbol{B}}_l$ is the unit vector along the local mean field.

Fig. 7(a) shows the contours obtained by the method for the high Mach-number run. In Fig. 7(b), we compare the result obtained this way (dashed lines) with our technique described in Section 2.3 (solid lines). We also show a similar plot for the mildly supersonic case in Fig. 7(c). These results confirm that the method described in Section 2.3 gives statistically correct scaling relations.

4 LINEAR ESTIMATES OF DENSITY AND MAGNETIC FIELD FLUCTUATIONS

In this section we estimate the magnitude of the rms fluctuations of magnetic field and density. Figs 3, 4 and 5 show that the magnetic field and density have spectral indexes similar to those of the velocity. We also expect that the isotropy/anisotropy of the magnetic field is similar to that of the velocity. Therefore, we do not discuss these quantities here. However, the anisotropy of the density shows different behaviour. Fig. 8 shows the structure of the density. The density shows anisotropy for the high-β case. But, for low-β cases, the density shows more or less isotropic structures. We suspect that shock formation is responsible for the isotropization of the density.

To estimate the rms fluctuations, we use the following linearized continuity and induction equations:

$$|\rho_k| = (\rho_0 v_k/c)|\hat{\boldsymbol{k}} \cdot \hat{\boldsymbol{\xi}}|, \tag{15}$$

$$|b_k| = (B_0 v_k/c)|\hat{\boldsymbol{B}}_0 \times \hat{\boldsymbol{\xi}}|, \tag{16}$$

where c denotes the propagation speed of the slow or fast wave (equation A22). From this, we obtain the rms fluctuations

$$(\delta\rho/\rho_0)_\mathrm{s} = (\delta V)_\mathrm{s} \langle |\hat{\boldsymbol{k}} \cdot \hat{\boldsymbol{\xi}}_\mathrm{s}/c_\mathrm{s}| \rangle, \tag{17}$$

$$(\delta\rho/\rho_0)_\mathrm{f} = (\delta V)_\mathrm{f} \langle |\hat{\boldsymbol{k}} \cdot \hat{\boldsymbol{\xi}}_\mathrm{f}/c_\mathrm{f}| \rangle, \tag{18}$$

$$(\delta B/B_0)_\mathrm{s} = (\delta V)_\mathrm{s} \langle |\hat{\boldsymbol{B}}_0 \times \hat{\boldsymbol{\xi}}_\mathrm{s}/c_\mathrm{s}| \rangle, \tag{19}$$

$$(\delta B/B_0)_\mathrm{f} = (\delta V)_\mathrm{f} \langle |\hat{\boldsymbol{B}}_0 \times \hat{\boldsymbol{\xi}}_\mathrm{f}/c_\mathrm{f}| \rangle, \tag{20}$$

where the angled brackets denote a proper Fourier space average. The generation of the slow- and fast-mode velocity ($(\delta V)_\mathrm{s}$ and $(\delta V)_\mathrm{f}$) depends on the driving force. Therefore, we may simply assume that

$$(\delta V)_\mathrm{A} \sim (\delta V)_\mathrm{s} \sim (\delta V)_\mathrm{f}, \tag{21}$$

where we ignore constants of order unity. However, when we consider mostly incompressible driving, the generation of fast modes

[7] One way to remove the effect of wandering field lines is to drive turbulence anisotropically in such a way that $k_{\perp,L}\delta V \sim k_{\parallel,L} V_\mathrm{A}$, where $k_{\perp,L}$ and $k_{\parallel,L}$ stand for the wavelengths of the driving scale and δV is the rms velocity. By increasing the $k_{\perp,L}/k_{\parallel,L}$ ratio, we can reduce the degree of mixing of different wave modes.

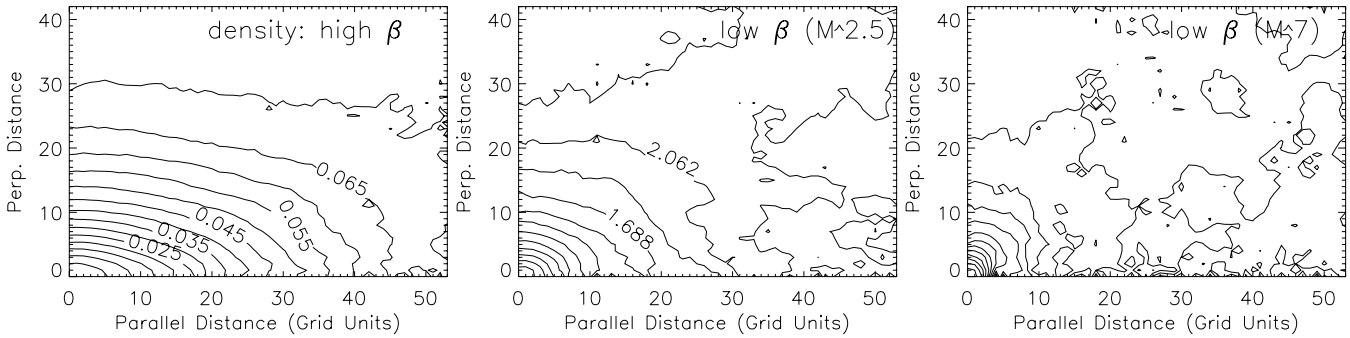

Figure 8. Density structures. (a) Left: $M_s \sim 0.35$ (high β). (b) Middle: $M_s \sim 2.3$ (mildly supersonic low β). (c) Right: $M_s \sim 7$ (highly supersonic low β).

follows equation (1). In this case, the amplitude of the fast-mode velocity is reduced by a factor of $[(V_A^2 + a^2)\,(\delta V)_A\,/(\delta V)_A^2\,V_A[^{-1/2}$:

$$(\delta V)_A \sim (\delta V)_s \sim \left[\frac{V_A^2 + a^2}{(\delta V)_A^2}\,\frac{(\delta V)_A}{V_A}\right]^{1/2} (\delta V)_f. \tag{22}$$

When we assume $(\delta V)_A \sim V_A$, equation (22) reduces to equation (21) in low-β plasmas.

4.1 Low-β case

In this limit, $c_s \sim a\cos\theta$ and $c_f \sim V_A$. Using equations (A31) and (A32), we obtain

$$(\delta\rho/\rho_0)_s \sim (\delta V)_s\langle|\cos\theta/c_s|\rangle \sim (\delta V)_s/a, \tag{23}$$

$$(\delta\rho/\rho_0)_f = (\delta V)_f\langle|\sin\theta/c_f|\rangle \sim (\delta V)_f/V_A, \tag{24}$$

$$(\delta B/B_0)_s = (\delta V)_s\langle|\alpha\cos\theta\sin\theta/c_s|\rangle \sim \alpha(\delta V)_s/a, \tag{25}$$

$$(\delta B/B_0)_f = (\delta V)_f\langle|1/c_f|\rangle \sim (\delta V)_f/V_A, \tag{26}$$

where we ignore the $\cos\theta$'s or $\sin\theta$'s.

When we assume $(\delta V)_A \sim (\delta V)_s \sim (\delta V)_f \sim V_A$, we get

$$(\delta\rho/\rho_0)_s \sim M_s, \tag{27}$$

$$(\delta\rho/\rho_0)_f = \sqrt{\beta}M_s, \tag{28}$$

$$(\delta B/B_0)_s = \beta M_s, \tag{29}$$

$$(\delta B/B_0)_f = \sqrt{\beta}M_s. \tag{30}$$

Therefore, in low-β plasmas, slow modes give rise to most of the density fluctuations (CL02). On the other hand, magnetic fluctuation by slow modes is smaller than that by fast modes by a factor of $\sqrt{\beta}$.

4.2 High-β case

In this limit, $c_s \sim V_A\cos\theta$ and $c_f \sim a$. Using equations (A33) and (A34), we obtain

$$\begin{aligned}(\delta\rho/\rho_0)_s &\sim (\delta V)_s\langle|\cos\theta\sin\theta/(\alpha c_s)|\rangle \\ &\sim (V_A/a)(\delta V)_s/a,\end{aligned} \tag{31}$$

$$(\delta\rho/\rho_0)_f = (\delta V)_f\langle|1/c_f|\rangle \sim (\delta V)_f/a, \tag{32}$$

$$(\delta B/B_0)_s = (\delta V)_s\langle|\cos\theta/c_s|\rangle \sim (\delta V)_s/V_A, \tag{33}$$

$$(\delta B/B_0)_f = (\delta V)_f\langle|\sin\theta/c_f|\rangle \sim (\delta V)_f/a, \tag{34}$$

where we ignore the $\cos\theta$'s or $\sin\theta$'s.

Let us just assume that $(\delta V)_A \sim (\delta V)_s \sim V_A \sim M_s^{-1}(\delta V)_f$ (cf. equation 22). Then we have

$$(\delta\rho/\rho_0)_s \sim M_s/\sqrt{\beta} \sim M_s^2, \tag{35}$$

$$(\delta\rho/\rho_0)_f \sim M_s^2, \tag{36}$$

$$(\delta B/B_0)_s = O(1), \tag{37}$$

$$(\delta B/B_0)_f = M_s^2. \tag{38}$$

The density fluctuation associated with slow modes is $\sim M_s^2$, when $(\delta V)_s \sim (\delta V)_A \sim V_A$. This is consistent with Zank & Matthaeus (1993). The ratio of $(\delta\rho)_s$ to $(\delta\rho)_f$ is of order unity. Therefore, both slow and fast modes give rise to similar amounts of density fluctuations. Note that this argument is of order-of-magnitude in nature. In fact, in our simulations for the high-β case, the rms density fluctuation by slow modes is about twice as large as that by fast modes. When we use equation (21), we have a different result: $(\delta\rho)_s \sim (V_A/a)(\delta\rho)_f < (\delta\rho)_f$. It is obvious that slow modes dominate magnetic fluctuations: $(\delta B)_s > (\delta B)_f$ for both equations (21) and (22).

5 VISCOSITY-DAMPED REGIME OF MHD TURBULENCE

In hydrodynamic turbulence viscosity sets a minimal scale for motion, with an exponential suppression of motion on smaller scales. Below the viscous cut-off the kinetic energy contained in a wavenumber band is dissipated at that scale, instead of being transferred to smaller scales. This means the end of the hydrodynamic cascade, but in MHD turbulence this is not the end of magnetic structure evolution. For viscosity much larger than resistivity, $\nu \gg \eta$, there will be a broad range of scales where viscosity is important but resistivity is not. On these scales magnetic field structures will be created by shear from non-damped turbulent motions, which amounts essentially to shear from the smallest undamped scales. The created magnetic structures would evolve through generating small-scale motions. As a result, we expect a power-law tail in the magnetic energy distribution, rather than an exponential cut-off. Cho, Lazarian & Vishniac (CLV02b) performed numerical simulations of turbulence in this regime threaded by a strong ($B_0/\sqrt{4\pi\rho} \sim \delta V$) mean magnetic field and reported that this regime possesses completely different scaling relations and anisotropic structures compared with ordinary MHD turbulence. Further research showed that there is a smooth connection between this regime and the small-scale turbulent dynamo in high magnetic Prandtl number fluids (see Schekochihin et al. 2002).[8]

[8] It is worth noting that, motivated by the analogy between time evolution equations for the magnetic field and for vorticity, Batchelor (1950) first

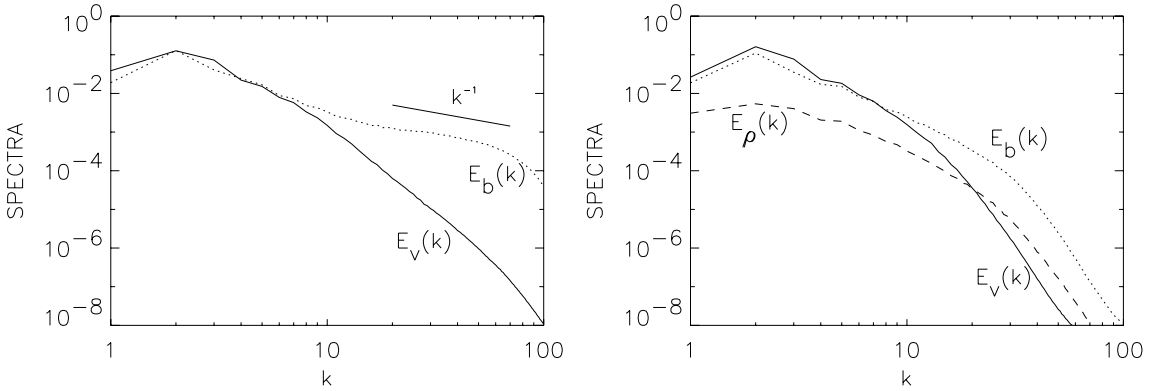

Figure 9. Viscous damped regime (viscosity > magnetic diffusivity). Due to large viscosity, velocity damps after $k \sim 10$. (a) Left: incompressible case with 384^3 grid points. Magnetic spectra show a shallower slope ($E_b(k) \propto k^{-1}$) below the velocity damping scale. We achieve a very small magnetic diffusivity through the use of hyper-diffusion. From Cho et al. (2002b). (b) Right: compressible case with 216^3 grid points. Magnetic and density spectra show structures below the velocity damping scale at $k \sim 10$. The structures are less obvious than the incompressible case because it is relatively hard to achieve very small magnetic diffusivity in the compressible run.

In partially ionized gas, neutrals produce viscous damping of turbulent motions. In a cold neutral medium (see Draine & Lazarian 1999, for a list of the idealized phases) this produces damping on the scale of a fraction of a parsec. The magnetic diffusion in these circumstances is still negligible and exerts an influence only at much smaller scales, ∼100 km. Therefore, there is a large range of scales where the physics of the turbulent cascade is very different from the conventional MHD turbulence picture.

CLV02b explored this regime numerically with a grid of 384^3 points and a physical viscosity for velocity damping. The kinetic Reynolds number was around 100. We achieved a very small magnetic diffusivity by the use of hyper-diffusion. The result is presented in Fig. 9(a). A theoretical model for this regime and its consequences for stochastic reconnection (Lazarian & Vishniac 1999) can be found in Lazarian, Vishniac & Cho (2003a). It explains the spectrum $E(k) \sim k^{-1}$ as a cascade of magnetic energy to small scales under the influence of shear at the marginally damped scales. The spectrum is similar to that of the passive scalar viscous–convective range in hydrodynamic turbulence (see, for example, Batchelor 1959; Lesieur 1990), although the study in Lazarian et al. (2003a) suggests that the physical origin of it is different. A study confirming that the k^{-1} spectrum is not a bottleneck effect is presented in Cho, Lazarian & Vishniac (2003c). The mechanism is based on the solenoidal motions and therefore the compressibility should not alter the physics of this regime of turbulence.

We show our results for the compressible fluid in Fig. 9(b). We use the same physical viscosity as in the incompressible case (see CLV02b). We rely on numerical diffusion, which is much smaller than physical viscosity, for the magnetic field. The inertial range is much smaller for numerical reasons, but it is clear that the viscosity-damped regime of MHD turbulence persists. The magnetic fluctuations, however, compress the gas and thus cause fluctuations in density. This is a new (although expected) phenomenon compared to our earlier incompressible calculations. These density fluctuations may have important consequences for the small-scale structure of the ISM.

argued that small magnetic fields can be amplified when viscosity is larger than magnetic diffusion (i.e. magnetic Prandtl number > 1). Although the analogy was later proved to be physically wrong, the high magnetic Prandtl number dynamo has been studied by many researchers (e.g. Kulsrud & Anderson 1992; Kinney et al. 2000).

6 ASTROPHYSICAL IMPLICATIONS OF OUR RESULTS

6.1 Parameter range explored

Parameters of astrophysical plasmas differ substantially for different astrophysical systems, from extremely high β to extremely low β. Turbulence in some systems is expected to be super-Alfvénic, in others it is expected to be sub-Alfvénic. Moreover, there is an ongoing controversy on what to expect and where. For instance, while high β was considered a default for many phases of the Milky Way ISM, recent observations by Beck (2002) suggest that the plasmas there may be low β. Therefore it is essential to have a clear understanding of MHD turbulence for as large a parameter space as possible.

Super-Alfvénic regime. We have argued above that the difference between super-Alfvénic and sub-Alfvénic turbulence is not as substantial as it is frequently thought. The difference between the two regimes stems from the ratio of the magnetic field to kinetic energies. However, as we mentioned in Section 2, if the kinetic energy density exceeds the magnetic field energy density, the hydromagnetic motions drive the turbulent dynamo. This enhances the magnetic field energy density up to approximately equipartition value. Thus the difference between the super-Alfvénic and sub-Alfvénic regimes amounts not to the energy of the magnetic field, but to the global level of field organization, e.g. to the magnetic field reversals, etc. Our results in Section 3.4 suggest that the basic properties of MHD turbulence in the sub-Alfvénic and super-Alfvénic regimes are similar. This, however, does not preclude the intermittency of MHD turbulence being very different. The latter property can be tested using scalings of the higher-order velocity correlations $\mathrm{SF}_p(\boldsymbol{r}) \equiv \langle |\boldsymbol{v}(\boldsymbol{x}+\boldsymbol{r}) - \boldsymbol{v}(\boldsymbol{x})|^p \rangle \propto r^{\zeta(p)}$. The corresponding scaling suggested by She & Leveque (1994) contains three parameters (see Politano & Pouquet 1995; Müller & Biskamp 2000): g is related to the scaling $\delta v_l \sim l^{1/g}$, x is related to the energy cascade rate $t_l^{-1} \sim l^{-x}$, and C to the codimension of the dissipative structures:

$$\zeta(p) = p/g(1-x) + C(1-(1-x/C)^{p/g}). \quad (39)$$

Müller & Biskamp (2000) proposed that 3D incompressible MHD turbulence for zero mean field has Kolmogorov g and x, while dissipation happens in sheet-like structures, i.e. $C = 3 - 2 = 1$. Using equation (39) they obtained an excellent fit for their incompress-

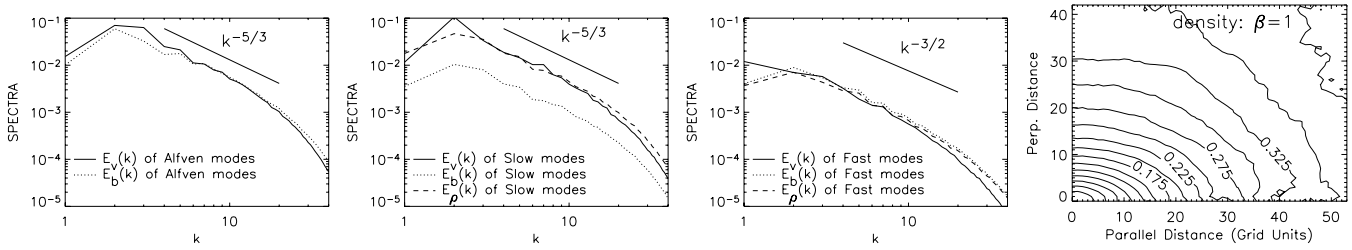

Figure 10. $\beta = 1$ case. (a) Left: Alfvén-mode spectra. (b) Second-left: slow-mode spectra. (c) Second-right: fast-mode spectra. (d) Right: density structure.

ible data. Later Boldyrev (2002) made the same assumption[9] that $C = 1$ (and same g and x) for compressible turbulence and Boldyrev et al. (2002a) obtained an excellent fit to their compressible data. It appears surprising that incompressible MHD (Müller & Biskamp 2000) and supersonic compressible MHD (Boldyrev et al. 2002a) have similar intermittency structures. This issue is discussed by Cho et al. (2003c).

We would like to note, however, that our considerations about super-Alfvénic turbulence are not applicable to transient regimes when super-Alfvénic motions are in the process of generating the magnetic field and the magnetic energy does not have time to come to a rough equipartition with the kinetic energy. Some parts of the ISM could well be in the transient regime for which temporarily $\rho V^2/2 \gg B^2/8\pi$.

$\beta = 1$ case. We provided theoretical considerations for both the $\beta \gg 1$ and $\beta \ll 1$ cases. What about the intermediate cases of $\beta \sim 1$? Would the scaling of modes and mode coupling be different? To test this case we performed calculations for $\beta = 1$. The results in Fig. 10 show that the scaling relations that hold true for the mildly low-β regime are also applicable for the $\beta = 1$ regime.

6.2 Fundamental questions

How fast does MHD turbulence decay? This question has fundamental implications for star formation (see McKee 1999). Indeed, it was thought originally that magnetic fields would prevent turbulence from fast decay. Later (see Mac Low et al. 1998; Stone, Ostriker & Gammie 1998; and the review by Vazquez-Semadeni et al. 2000b) this was reported not to be true. However, fast decay was erroneously associated with the coupling between compressible and incompressible modes. The idea was that incompressible motions quickly transfer their energy to the compressible modes, which are rapidly damped by direct dissipation (presumably through shock formation).

Our calculations support the conjecture given by equation (1). According to this, the coupling of Alfvén and compressible motions is important only at the energy injection scales where $\delta V_l \sim V_A$. As the turbulence evolves the perturbations become smaller and the coupling less efficient. Typically for numerical simulations the inertial range is rather small and this could explain why marginal coupling of modes was not noticed.

Our results show that MHD turbulence damping does not depend on whether the fluid is compressible or not. The incompressible motions damp also within one eddy turn-over time.[10] This is a consequence of the fact that within strong turbulence,[11] mixing motions perpendicular to the magnetic field are hydrodynamic to high order (CLV02a) and the cascade of energy induced by these motions is similar to the hydrodynamic cascade, i.e. an energy cascade happens within an eddy turn-over time.

The reported (see Mac Low et al. 1998) decay of the total energy of turbulent motions $E_{\rm tot}$ follows t^{-1} which can be understood if we account for the fact that the energy is being injected at a scale smaller than the scale of the system. Therefore some energy originally diffuses to larger scales through the inverse cascade. Our calculations, stimulated by illuminating discussions with Chris McKee, show that if this energy transfer is artificially prevented by injecting the energy on the scale of the computational box, the scaling of $E_{\rm tot}$ becomes closer to t^{-2}.

Can compressible MHD turbulence decay slowly? Incompressible MHD computations (see Maron & Goldreich 2001, CLV02a) show that the rate of turbulence decay depends on the degree of turbulence imbalance,[12] i.e. the difference in the energy fluxes moving in opposite directions. Strongly imbalanced incompressible turbulence was shown to persist longer than its balanced counterpart. This enabled CLV02a to speculate that this may allow energy transfer between clouds and may explain the observed turbulent linewidths of GMCs without evident star formation. Imbalanced turbulence can also make it possible to transfer energy from the galactic disc to heat the Reynolds layer (see Reynolds 1988).

Our results above show a marginal coupling of compressible and incompressible modes. This suggests that the results obtained in incompressible simulations are applicable to compressible environments if the amplitudes of perturbations are not large. The complication arises from the existence of the parametric instability (Del Zanna, Velli & Londrillo 2001) that happens as the density perturbations reflect Alfvén waves and grow in amplitude. This instability eventually controls the degree of imbalance that is achievable. However, the growth rate of the instability is substantially slower than the Alfvén wave oscillation rate. Therefore, if we take into account that interstellar sources are intermittent not only in space, but also in time, the transport of turbulent energy described in CLV02a seems

[9] The physical motivation of Müller & Biskamp (2000) and Boldyrev (2002) for choosing the same value of C are different, however. Boldyrev (2002) identifies the dissipation structures with shocks, which are absent in the incompressible simulations by Müller & Biskamp (2000).

[10] It is generally believed that the decay of turbulence energy follows a power law. A possible expression is $E(t) \sim E_0/[1 + C(t - t_0)]^n$ (C. McKee, private communication), where E_0 is the energy at the initial time t_0. Our claim is that the decay of turbulence follows $E(t) \sim E_0/[1 + C'(t - t_0)/t_{\rm cas,0}]^n$, where $t_{\rm cas,0}$ is the eddy turn-over time at $t = t_0$ and C' is a constant of order unity.

[11] For a formal definition of strong, weak and intermediate turbulence, see Goldreich & Sridhar (1997) and CLV03a, but here we just mention in passing that in most astrophysically important cases the MHD turbulence is 'strong'.

[12] This quantity is also called cross-helicity (see Matthaeus, Goldstein & Montgomery 1983).

feasible. Here we mention that the growth of the parametric instability described above may provide an alternative explanation for the observed infall motions of the cloud cores (Tafalla et al. 1998). Earlier, these motions were explained as arising from linear damping of Alfvén waves (Myers & Lazarian 1998).

Is the correlation between magnetic field and density tight in MHD turbulence? In the traditional static paradigm of the ISM, the density and magnetic field increase simultaneously as clouds contract. The introduction of turbulence into the picture of the ISM complicates the analysis (see the discussion in Vazquez-Semadeni et al. 2000b; CLV03a). Our results confirm earlier claims (e.g. Passot & Vazquez-Semadeni 2003) that magnetic field–density correlations may be weak. First of all, some magnetic field fluctuations are related to Alfvénic turbulence which does not compress the medium. Second, slow modes in low-β plasmas are essentially density perturbations that propagate along the magnetic field and which marginally perturb magnetic fields. Moreover, our calculations (see Fig. 8) show that at substantially high Mach numbers the density correlations do not show anisotropies, while magnetic field fluctuations are anisotropic. On the basis of our calculations we might expect that the correlation may be a bit higher for high-β than for low-β plasmas.

Can viscously damped turbulence explain tiny-scale atomic structures? The term 'tiny-scale atomic structures' (TSAS) was introduced by Heiles (1997) to describe the mysterious H I absorbing structures on scales from thousands to tens of AUs, discovered by Dieter, Welch & Romney (1976). Analogues of TSAS are observed in Na I and Ca II (Meyer & Blades 1996; Andrews, Meyer & Lauroesch 2001; Faison & Goss 2001) and in molecular gas (Marscher, Moore & Bania 1993).

These structures can be produced by turbulence with a spectrum substantially shallower than the Kolmogorov spectrum, e.g. with the spectrum $E(k) \sim k^{-1}$ (see Deshpande 2000). Simulations in CLV02b and theoretical calculations in Lazarian et al. (2003a) show that the magnetic field in the viscosity-damped regime of MHD turbulence (see Section 5) can produce such a spectrum of magnetic fluctuations. Our calculations above are indicative that this will translate into the corresponding shallow spectrum of the density. Our calculations are applicable on scales from the viscous damping scale (determined by equating the energy transfer rate with the viscous damping rate; $\sim$0.1 pc in a warm neutral medium with $n = 0.4$ cm^{-3}, $T = 6000$ K) to the ion–neutral decoupling scale (the scale at which viscous drag on ions becomes comparable to neutral drag; $\ll$0.1 pc). Below the viscous scale the fluctuations of the magnetic field obey the damped regime shown in Fig. 9(b) and produce density fluctuations. For a typical cold-neutral-medium gas, the scale of neutral–ion decoupling decreases to $\sim$70 AU, and is less for denser gas. TSAS may be created by strongly non-linear MHD turbulence!

6.3 Application of the scaling laws obtained

Many astrophysical problems require some knowledge of the scaling properties of turbulence. Therefore we expect a wide range of applications of the established scaling relations. Here we discuss how our understanding of MHD turbulence affects a few selected issues.

As we mentioned in the introduction, the observations (see CLV03a for a review) indicate that the interstellar spectrum exhibits Kolmogorov-type scaling $E(k) \sim k^{-5/3}$. On the basis of what we have learned by now (see also Higdon 1984, GS95, Lithwick & Goldreich 2001, CL02) we may conclude that the MHD spectrum is different from the spectrum of isotropic Kolmogorov turbulence. The anisotropy of Alfvénic and slow modes ensures that the observationally measured spectrum is dominated by perturbations perpendicular to the magnetic field, i.e. $E(k) \sim k_\perp^{-5/3}$. Admixture of fast modes can alter the spectrum, but observations indicate that these modes do not dominate the detected signal.

Whether or not one can use Kolmogorov isotropic scaling for practical calculations depends on the nature of the problem. For instance, Cho & Lazarian (2002b) use Kolmogorov scaling to calculate the spectra of fluctuations arising from synchrotron emission and of fluctuations of the degree of starlight polarization and obtained good correspondence with the observed statistics. However, for many problems turbulence anisotropy is essential.

Cosmic rays. The propagation of cosmic rays is mainly determined by their interactions with electromagnetic fluctuations in the interstellar medium. For practical calculations it is usually assumed that the turbulence is isotropic with a Kolmogorov spectrum (e.g. Schlickeiser & Miller 1998). How should these calculations be modified in view of our findings? Chandran (2000) and Yan & Lazarian (2002) (see also Lazarian, Cho & Yan 2002, for a review) calculated the efficiency of cosmic ray scattering by Alfvénic modes and found that, if the energy is injected at large scales, the scattering by Alfvénic modes is absolutely negligible. The difference between the calculations in Yan & Lazarian (2002), which used the tensor description of Alfvén waves obtained in CLV02a, and the calculations that use Kolmogorov turbulence was 10 orders of magnitude! Yan & Lazarian (2002, 2003a) identified fast modes as the principal source of cosmic ray scattering and used the CL02 results to calculate the scattering rate in low-β plasmas. Damping of those modes, however, depends on the value of β, which entails the dependence of cosmic ray scattering on the temperature and density of the background plasmas.

Dust dynamics. Turbulence induces relative dust grain motions and leads to grain–grain collisions. These collisions determine the grain size distribution, which affects most dust properties, including absorption and H_2 formation. Unfortunately, as in the case of cosmic rays, earlier work appealed to hydrodynamic turbulence to predict grain relative velocities. Lazarian & Yan (2002) and Yan & Lazarian (2003b) considered motions of charged grains in anisotropic MHD turbulence and found that the direct interaction of the charged grains with the turbulent magnetic field results in a stochastic acceleration that can potentially provide grains with supersonic velocities.

Other applications. The obtained scaling laws are essential for understanding the density fluctuations within H II regions (Lithwick & Goldreich 2001), stochastic magnetic reconnection in fully ionized (Lazarian & Vishniac 1999, 2000) and partially ionized plasmas (Lazarian et al. 2003a), for energy transfer to electrons in gamma ray bursts and solar flares (see Lazarian et al. 2003b). This list can be easily extended.

7 SUMMARY

In this paper, we have studied the statistics of compressible MHD turbulence for high-, intermediate- and low-β plasmas and for different sonic and Alfvén Mach numbers. For sub-Alfvénic turbulence we provided the decomposition of turbulence into Alfvén, slow and fast modes. We have found that the coupling of compressible and incompressible modes is weak and, contrary to the common belief, the drain of energy from Alfvén to compressible modes is marginal along the cascade. For the cases studied, we have found that GS95

scaling is valid for Alfvén modes:

Alfvén: $E^A(k) \propto k^{-5/3}, k_\parallel \propto k_\perp^{2/3}$.

Slow modes also follow the GS95 model for both high-β and mildly supersonic low-β cases:

Slow: $E^s(k) \propto k^{-5/3}, k_\parallel \propto k_\perp^{2/3}$.

For the highly supersonic low-β case, the kinetic energy spectrum of slow modes tends to be steeper, which may be related to the formation of shocks.

Fast mode spectra are compatible with acoustic turbulence scaling relations:

Fast: $E^f(k) \propto k^{-3/2}$, isotropic spectrum.

Our super-Alfvénic turbulence simulations suggest that the picture above holds true at sufficiently small scales at which the Alfvén speed V_A is larger than the turbulent velocity v_l. This part of our study shows that compressible MHD turbulence is not a mess. On the contrary, its statistics obey well-determined universal scaling relations. The importance of these relations for different branches of astrophysics is obvious.

Addressing the issue of MHD turbulence damping in partially ionized gas we showed that the viscosity-damped regime of MHD turbulence below the viscous damping scale that was reported in CLV02b for an incompressible fluid persists when compressibility is present. The spectrum of density fluctuations that we obtain may be related to the mysterious tiny-scale structures observed in the ISM.

ACKNOWLEDGMENTS

We thank Ethan Vishniac, Peter Goldreich, Bill Matthaeus, Chris McKee, and Annick Pouquet for stimulating discussions. We acknowledge the support of NSF Grant AST-0125544. This work was partially supported by NCSA under AST010011N and utilized the NCSA Origin2000.

REFERENCES

Andrews S. M., Meyer D. M., Lauroesch J. T., 2001, ApJ, 552, L73
Armstrong J. W., Rickett B. J., Spangler S. R., 1995, ApJ, 443, 209
Batchelor G. K., 1950, Proc. Roy. Soc. Lond., A, 201, 405
Batchelor G. K., 1959, J. Fluid Mech., 5, 113
Beck R., 2002, preprint (astro-ph/0212288)
Bertoglio J.-P., Bataille F., Marion J.-D., 2001, Phys. Fluids, 13, 290
Boldyrev S., 2002, ApJ, 569, 841
Boldyrev S., Nordlund Å., Padoan P., 2002a, ApJ, 573, 678
Boldyrev S., Nordlund Å., Padoan P., 2002b, Phys. Rev. Lett., 89, 031102
Brandenburg A., Jennings R., Nordlund A., Rieutord M., Stein R., Tuominen I., 1996, J. Fluid Mech., 306, 325
Chandran B., 2000, Phys. Rev. Lett., 85, 4656
Cho J., Lazarian A., 2002a, Phy. Rev. Lett., 88, 245001 (CL02)
Cho J., Lazarian A., 2002b, ApJ, 575, L63
Cho J., Vishniac E., 2000b, ApJ, 539, 273
Cho J., Vishniac E., 2000a, ApJ, 538, 217
Cho J., Lazarian A., Vishniac E., 2002a, ApJ, 564, 291 (CLV02a)
Cho J., Lazarian A., Vishniac E., 2002b, ApJ, 566, L49 (CLV02b)
Cho J., Lazarian A., Vishniac E., 2003a, in Falgarone E., Passot T., eds, Turbulence and Magnetic Fields in Astrophysics. Springer LNP, Berlin, p. 56 (CLV03a)
Cho J., Lazarian A., Honein A., Knaepen B., Kassinos S., Moin P., 2003b, ApJ, 589, L77
Cho J., Lazarian A., Vishniac E., 2003, ApJ, in press (astro-ph/0305212)
Del Zanna L., Velli M., Londrillo P., 2001, A&A, 367, 705
Deshpande A. A., 2000, MNRAS, 317, 199
Deshpande A. A., Dwarakanath K. S., Goss W. M., 2000, ApJ, 543, 227
Dieter N. H., Welch W. J., Romney J. D., 1976, ApJ, 206, L113
Draine B. T., Lazarian A., 1999, ApJ, 512, 740
Faison M. D., Goss W. M., 2001, AJ, 121, 2706
Goldreich P., Sridhar S., 1995, ApJ, 438, 763
Goldreich P., Sridhar S., 1997, ApJ, 485, 680
Heiles C., 1997, ApJ, 481, 193
Higdon J. C., 1984, ApJ, 285, 109
Kida S., Yanase S., Mizushima J., 1991, Phys. Fluids A, 3, 457
Kinney R. M., Chandran B., Cowley S., McWilliams J. C., 2000, ApJ, 545, 907
Kolmogorov A., 1941, Dokl. Akad. Nauk SSSR, 31, 538
Kulsrud R., Anderson S., 1992, ApJ, 396, 606
Lazarian A., Cho J., Yan H., 2002, preprint (astro-ph/0211031)
Lazarian A., Esquivel E., 2003, ApJ, 592, L37
Lazarian A., Pogosyan D., 2000, ApJ, 537, 720
Lazarian A., Vishniac E. T., 1999, ApJ, 517, 700
Lazarian A., Vishniac E. T., 2000, Rev. Mex. Astron. Astrofis., 9, 55
Lazarian A., Vishniac E. T., Cho J., 2003a, ApJ, submitted
Lazarian A., Petrosian V., Yan H., Cho J., 2003b, preprint (astro-ph/0301181)
Lazarian A., Yan H., 2002, ApJ, 566, L105
Leamon R. J., Smith C. W., Ness N. F., Matthaeus W. H., Wong H., 1998, J. Geophys Res., 103, 4775
Lesieur M., 1990, Turbulence in Fluids. Kluwer, Dordrecht
Lithwick Y., Goldreich P., 2001, ApJ, 562, 279
Liu X., Osher S., 1988, J. Comp. Phys., 141, 1
L'vov V. S., L'vov Y. V., Pomyalov A., 2000, Phys. Rev. E, 61, 2586
McKee C. F., 1999, in Charles J. L., Nikolaos D. K., eds, The Origin of Stars and Planetary Systems. Kluwer, Dordrecht, p. 29
Mac Low M.-M., Klessen R., Burkert A., Smith M., 1998, Phy. Rev. Lett., 80, 2754
Maron J., Goldreich P., 2001, ApJ, 554, 1175
Marscher A. P., Moore E. M., Bania T. M., 1993, ApJ, 419, L101
Matthaeus W. H., Brown M. R., 1988, Phys. Fluids, 31(12), 3634
Matthaeus W. H., Ghosh S., Oughton S., Roberts D. A., 1996, J. Geophysical Res., 101(A4), 7619
Matthaeus W. H., Goldstein M. L., Montgomery D. C., 1983, Phys. Rev. Lett., 51, 1484
Meyer D. M., Blades J. C., 1996, ApJ, 464, L179
Monin A. S., Yaglom A. A., 1975, Statistical Fluid Mechanics: Mechanics of Turbulence, Vol. 2. MIT Press, Cambridge MA
Myers P., Lazarian A., 1998, ApJ, 507, 157
Müller W.-C., Biskamp D., 2000, Phys. Rev. Lett., 84(3), 475
Padoan P., Nordlund A., 1999, ApJ, 526, 279
Passot T., Vazquez-Semadeni E., 2003, A&A, 398, 845
Politano H., Pouquet A., 1995, Phy. Rev. E, 52, 636
Porter D., Pouquet A., Woodward P., 2002, Phys. Rev. E, 66, 026301
Reynolds R. J., 1988, ApJ, 333, 341
Schekochihin A., Maron J., Cowley S., McWilliams J., 2002, ApJ, 576, 806
Schlickeiser A., Miller J. A., 1998, ApJ, 492, 352
She Z., Leveque E., 1994, Phy. Rev. Lett., 72, 336
Shebalin J. V., Matthaeus W. H., Montgomery D. C., 1983, J. Plasma Phys., 29, 525
Spangler S. R., 1991, ApJ, 376, 540
Spangler S. R., 1999, ApJ, 522, 879
Stanimirovic S., Lazarian A., 2001, ApJ, 551, L53
Stone J., Ostriker E., Gammie C., 1998, ApJ, 508, L99
Tafalla M., Mardones D., Myers P., Caselli P., Bachiller R., Benson B., 1998, ApJ, 504, 900
Thompson W. B., 1962, An Introduction to Plasma Physics. Pergamon Press, Oxford
Vazquez-Semadeni E., Ostriker E. C., Passot T., Gammie C. F., Stone J. M., 2000b, in Mannings V., Boss A.P., Russell S.S., eds, Protostars and Planets IV. Univ. Arisona Press, Tucson, p. 3
Yan H., Lazarian H., 2002, Phy. Rev. Lett., 89, 281102
Yan H., Lazarian H., 2003a, ApJ, 592, L33
Yan H., Lazarian H., 2003b, ApJ, submitted

Zakharov V. E., 1967, Sov. Phys. JETP, 24, 455
Zakharov V. E., Sagdeev A., 1970, Sov. Phys. Dokl., 15, 439
Zank G. P., Matthaeus W. H., 1993, Phys. Fluids A, 5(1), 257

APPENDIX A: MODE DECOMPOSITION

Let us consider a small perturbation in the presence of a strong mean magnetic field. We write the density, velocity, pressure, and magnetic field as the sum of constant and fluctuating parts: $\rho \rightarrow \rho_0 + \rho$, $\boldsymbol{v} \rightarrow \boldsymbol{v}_0 + \boldsymbol{v}$, $P \rightarrow P_0 + p$, and $\boldsymbol{B} \rightarrow \boldsymbol{B}_0 + \boldsymbol{b}$, respectively. We assume that $\boldsymbol{v}_0 = 0$ and that the perturbation is small: $\rho \ll \rho_0$, etc. Ignoring the second- and higher-order contributions, we can rewrite the MHD equations as follows:

$$\frac{\partial \rho}{\partial t} + \rho_0 \nabla \cdot \boldsymbol{v} = 0, \tag{A1}$$

$$\rho_0 \frac{\partial \boldsymbol{v}}{\partial t} + \nabla(a^2 \rho) - \frac{1}{4\pi}(\nabla \times \boldsymbol{b}) \times \boldsymbol{B}_0 = 0, \tag{A2}$$

$$\frac{\partial \boldsymbol{b}}{\partial t} + \nabla \times [\boldsymbol{v} \times \boldsymbol{B}_0] = 0, \tag{A3}$$

where we assume a polytropic equation of state: $p = a^2\ \rho$ with $a^2 = \gamma\, p_0/\rho_0$. We follow the arguments in Thompson (1962) to derive magnetosonic waves. Let $\boldsymbol{\xi}(\boldsymbol{r}, t)$ be the displacement vector, so that $\partial \boldsymbol{\xi}/\partial t = \boldsymbol{v}$. Assuming that the displacements vanish at $t = 0$, we can integrate the equations as follows

$$\rho + \rho_0 \nabla \cdot \boldsymbol{\xi} = 0, \tag{A4}$$

$$\ddot{\boldsymbol{\xi}} = a^2 \nabla(\nabla \cdot \boldsymbol{\xi}) + (\nabla \times \boldsymbol{b}) \times \boldsymbol{B}_0/4\pi\rho_0, \tag{A5}$$

$$\boldsymbol{b} = \nabla \times (\xi \times \boldsymbol{B}_0). \tag{A6}$$

The momentum equation (equation A5) becomes

$$\begin{aligned}\ddot{\boldsymbol{\xi}} &= a^2 \nabla(\nabla \cdot \boldsymbol{\xi}) + [\nabla \times (\nabla \times (\xi \times \boldsymbol{B}_0))] \times \boldsymbol{B}_0/4\pi\rho_0 \\ &= a^2 \nabla(\nabla \cdot \boldsymbol{\xi}) + \nabla\left(B_0^2 \nabla \cdot \boldsymbol{\xi} - \boldsymbol{B}_0 \cdot \nabla \boldsymbol{B}_0 \cdot \boldsymbol{\xi}\right)/4\pi\rho_0 \\ &\quad - (\boldsymbol{B}_0 \cdot \nabla)^2 \boldsymbol{\xi}/4\pi\rho_0 + [\boldsymbol{B}_0(\boldsymbol{B}_0 \cdot \nabla)\nabla \cdot \boldsymbol{\xi}]/4\pi\rho_0\end{aligned} \tag{A7}$$

Using $\alpha = a^2/V_{\rm A}^2 = \beta(\gamma/2)$, $V_{\rm A} = B_0/4\pi\rho_0$, we have

$$\begin{aligned}&\ddot{\boldsymbol{\xi}}/V_{\rm A}^2 - \nabla[(\alpha + 1)\nabla \cdot \boldsymbol{\xi} - (\hat{\boldsymbol{B}}_0 \cdot \nabla)(\hat{\boldsymbol{B}}_0 \cdot \boldsymbol{\xi})] \\ &\quad - (\hat{\boldsymbol{B}}_0 \cdot \nabla)^2 \boldsymbol{\xi} + (\hat{\boldsymbol{B}}_0 \cdot \nabla)(\nabla \cdot \boldsymbol{\xi})\hat{\boldsymbol{B}}_0 = 0.\end{aligned} \tag{A8}$$

In Fourier space the equation becomes

$$\ddot{\boldsymbol{\xi}}/V_{\rm A}^2 + k\hat{\boldsymbol{k}}[(\alpha + 1)k\xi_k - k_\parallel \xi_\parallel] + k_\parallel^2 \boldsymbol{\xi} - k_\parallel k \xi_k \hat{k}_\parallel = 0, \tag{A9}$$

where $\xi_k = \boldsymbol{\xi} \cdot \hat{\boldsymbol{k}}, \xi_\parallel = \boldsymbol{\xi} \cdot \hat{\boldsymbol{k}}_\parallel, \hat{\boldsymbol{k}} = \boldsymbol{k}/k$, and $\hat{\boldsymbol{k}}_\parallel$ is a unit vector parallel to $\boldsymbol{B}_0$ (i.e. $\hat{\boldsymbol{k}}_\parallel = \hat{\boldsymbol{B}}_0$). Assuming $\ddot{\boldsymbol{\xi}} = -\omega^2 \boldsymbol{\xi} = -c^2 k^2 \boldsymbol{\xi}$, we can rewrite (A9) as

$$\left(c^2/V_{\rm A}^2 - \cos^2\theta\right)\boldsymbol{\xi} - [(\alpha + 1)\xi_k - \cos\theta\xi_\parallel]\hat{\boldsymbol{k}} + \cos\theta\xi_k\hat{k}_\parallel = 0, \tag{A10}$$

where $\cos\theta = k_\parallel/k$ and θ is the angle between $\boldsymbol{k}$ and $\boldsymbol{B}_0$.

Using $\hat{\boldsymbol{k}} = \sin\theta\hat{\boldsymbol{k}}_\perp + \cos\theta\hat{\boldsymbol{k}}_\parallel$, we get

$$\begin{aligned}&\left(c^2/V_{\rm A}^2 - \cos^2\theta\right)\boldsymbol{\xi} - [(\alpha + 1)\xi_k - \cos\theta\xi_\parallel]\sin\theta\hat{\boldsymbol{k}}_\perp \\ &\quad -\{[(\alpha + 1)\xi_k - \cos\theta\xi_\parallel]\cos\theta - \cos\theta\xi_k\}\hat{\boldsymbol{k}}_\parallel = 0.\end{aligned} \tag{A11}$$

Writing $\boldsymbol{\xi} = \xi_\perp\hat{\boldsymbol{k}}_\perp + \xi_\parallel\hat{\boldsymbol{k}}_\parallel + \xi_\varphi\hat{\boldsymbol{\varphi}}$, we get

$$\left(c^2/V_{\rm A}^2 - \cos^2\theta\right)\xi_\perp - [(\alpha + 1)\xi_k - \cos\theta\xi_\parallel]\sin\theta = 0, \tag{A12}$$

$$\left(c^2/V_{\rm A}^2 - \cos^2\theta\right)\xi_\parallel - [\alpha\xi_k - \cos\theta\xi_\parallel]\cos\theta = 0, \tag{A13}$$

$$\left(c^2/V_{\rm A}^2 - \cos^2\theta\right)\xi_\varphi = 0. \tag{A14}$$

The non-trivial solution of equation (A14) is the Alfvén wave, whose dispersion relation is $\omega/k = V_{\rm A}\cos\theta$. The direction of the displacement vector for the Alfvén wave is parallel to the azimuthal basis $\hat{\boldsymbol{\varphi}}$:

$$\hat{\boldsymbol{\xi}}_{\rm A} = -\hat{\boldsymbol{\varphi}} = \hat{\boldsymbol{k}}_\perp \times \hat{\boldsymbol{k}}_\parallel. \tag{A15}$$

Let us consider solutions of equations (A12) and (A13). Using $\xi_k = \xi_\perp \sin\theta + \xi_\parallel \cos\theta$, we get

$$\left(c^2/V_{\rm A}^2 - \cos^2\theta\right)\xi_\perp - (\alpha + 1)\sin^2\theta\xi_\perp - \alpha\cos\theta\sin\theta\xi_\parallel = 0, \tag{A16}$$

$$\left(c^2/V_{\rm A}^2 - \cos^2\theta\right)\xi_\parallel - \alpha\sin\theta\cos\theta\xi_\perp - (\alpha - 1)\cos^2\theta\xi_\parallel = 0. \tag{A17}$$

Rearranging these, we get

$$\left(c^2/V_{\rm A}^2 - \alpha\sin^2\theta - 1\right)\xi_\perp - \alpha\cos\theta\sin\theta\xi_\parallel = 0, \tag{A18}$$

$$\left(c^2/V_{\rm A}^2 - \alpha\cos^2\theta\right)\xi_\parallel - \alpha\sin\theta\cos\theta\xi_\perp = 0. \tag{A19}$$

Combining these two, we get

$$\left(c^2/V_{\rm A}^2 - \alpha\sin^2\theta - 1\right)\left(c^2/V_{\rm A}^2 - \alpha\cos^2\theta\right) = \alpha^2\sin^2\theta\cos^2\theta. \tag{A20}$$

Therefore, the dispersion relation is

$$c^4/V_{\rm A}^4 - (1 + \alpha)c^2/V_{\rm A}^2 + \alpha\cos^2\theta = 0. \tag{A21}$$

The roots of the equation are

$$c_{\rm f,s}^2 = \frac{1}{2}V_{\rm A}^2[(1 + \alpha) \pm \sqrt{(1 + \alpha)^2 - 4\alpha\cos^2\theta}], \tag{A22}$$

where the subscripts 'f' and 's' stand for 'fast' and 'slow' waves, respectively.

We can write

$$\boldsymbol{\xi} = \xi_\parallel\hat{\boldsymbol{k}}_\parallel + \xi_\perp\hat{\boldsymbol{k}}_\perp \propto \left[\frac{\xi_\parallel k_\perp}{\xi_\perp k_\parallel}\right]k_\parallel\hat{\boldsymbol{k}}_\parallel + k_\perp\hat{\boldsymbol{k}}_\perp. \tag{A23}$$

Substituting equation (A22) into equations (A18) and (A19), we get

$$\left[\frac{1 + \alpha}{2} \pm \frac{\sqrt{D}}{2} - \alpha\sin^2\theta - 1\right]\xi_\perp = \alpha\cos\theta\sin\theta\xi_\parallel, \tag{A24}$$

$$\left[\frac{1 + \alpha}{2} \pm \frac{\sqrt{D}}{2} - \alpha\cos^2\theta\right]\xi_\parallel = \alpha\cos\theta\sin\theta\xi_\perp, \tag{A25}$$

where $D = (1 + \alpha)^2 - 4\alpha\cos^2\theta$. Using $k_\parallel = k\cos\theta$ and $k_\perp = k\cos\theta$, we get

$$\left[\frac{-1 + \alpha}{2} \pm \frac{\sqrt{D}}{2}\right]\xi_\perp k_\parallel - \alpha\sin^2\theta\xi_\perp k_\parallel = \alpha\cos^2\theta\xi_\parallel k_\perp, \tag{A26}$$

$$\left[\frac{1 + \alpha}{2} \pm \frac{\sqrt{D}}{2}\right]\xi_\parallel k_\perp - \alpha\cos^2\theta\xi_\parallel k_\perp = \alpha\sin^2\theta\xi_\perp k_\parallel. \tag{A27}$$

Rearranging these, we get

$$\frac{\xi_\parallel k_\perp}{\xi_\perp k_\parallel} = \frac{-1 + \alpha \pm \sqrt{D}}{1 + \alpha \pm \sqrt{D}}, \tag{A28}$$

where the upper signs are for the fast mode and the lower signs for the slow mode. Therefore, we get

$$\hat{\boldsymbol{\xi}}_{\rm s} \propto (-1 + \alpha - \sqrt{D})k_\parallel\hat{\boldsymbol{k}}_\parallel + (1 + \alpha - \sqrt{D})k_\perp\hat{\boldsymbol{k}}_\perp, \tag{A29}$$

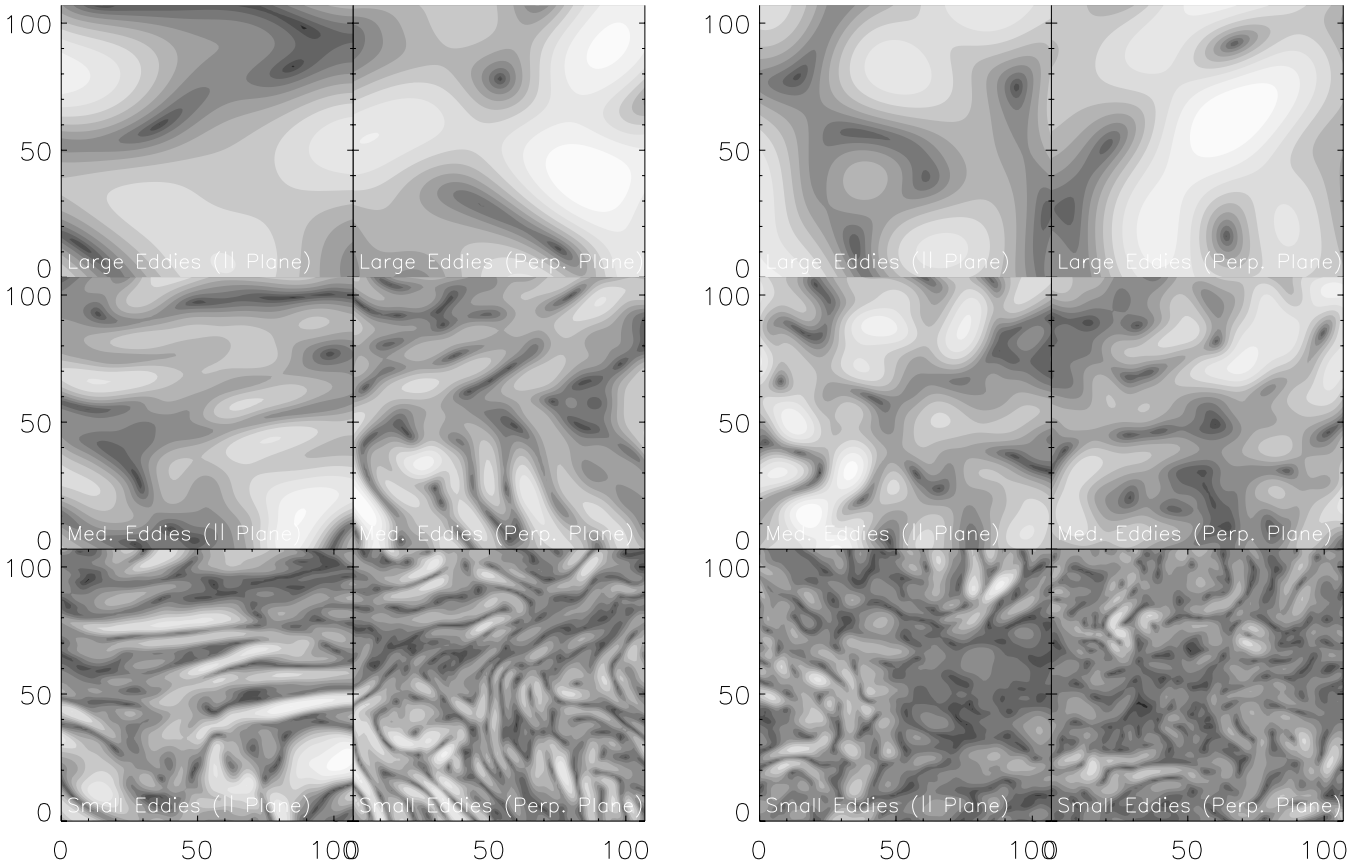

Figure B1. Anisotropy as a function of scale. Left: Alfvén-mode velocity shows scale-dependent anisotropy. Right: Fast-mode velocity shows isotropy. Only part of the data cube is shown. Lighter tones are for larger $|\boldsymbol{v}|$. The magnetic field shows similar behaviour.

$$\hat{\boldsymbol{\xi}}_{\rm f} \propto (-1+\alpha+\sqrt{D})k_{\parallel}\hat{\boldsymbol{k}}_{\parallel} + (1+\alpha+\sqrt{D})k_{\perp}\hat{\boldsymbol{k}}_{\perp}. \tag{A30}$$

The slow basis $\hat{\boldsymbol{\xi}}_{\rm s}$ lies between $\hat{\boldsymbol{k}}_{\parallel}$ and $-\hat{\boldsymbol{\theta}}$. The slow basis $\hat{\boldsymbol{\xi}}_{\rm f}$ lies between $\hat{\boldsymbol{k}}_{\perp}$ and $\hat{\boldsymbol{k}}$ (Fig. 1). Here the overall sign of $\hat{\boldsymbol{\xi}}_{\rm s}$ and $\hat{\boldsymbol{\xi}}_{\rm f}$ is not important.

When $\alpha \to 0$, equations (A30) and (A29) become

$$\hat{\boldsymbol{\xi}}_{\rm s} \approx \hat{\boldsymbol{k}}_{\parallel} - (\alpha \sin\theta\cos\theta)\hat{\boldsymbol{k}}_{\perp}, \tag{A31}$$

$$\hat{\boldsymbol{\xi}}_{\rm f} \approx (\alpha \sin\theta\cos\theta)\hat{\boldsymbol{k}}_{\parallel} + \hat{\boldsymbol{k}}_{\perp}. \tag{A32}$$

In this limit, $\hat{\boldsymbol{\xi}}_{\rm s}$ is mostly proportional to $\hat{\boldsymbol{k}}_{\parallel}$ and $\hat{\boldsymbol{\xi}}_{\rm f}$ to $\hat{\boldsymbol{k}}_{\perp}$. When $\alpha \to \infty$, equations (A30) and (A29) become

$$\hat{\boldsymbol{\xi}}_{\rm s} \approx -\hat{\boldsymbol{\theta}} + (\sin\theta\cos\theta/\alpha)\hat{\boldsymbol{k}}, \tag{A33}$$

$$\hat{\boldsymbol{\xi}}_{\rm f} \approx (\sin\theta\cos\theta/\alpha)\hat{\boldsymbol{\theta}} + \hat{\boldsymbol{k}}. \tag{A34}$$

When $\alpha = \infty$, the slow modes are called pseudo-Alfvénic modes.

We can obtain the slow and fast velocity components by projecting the Fourier velocity component $\boldsymbol{v}_{\boldsymbol{k}}$ on to $\hat{\boldsymbol{\xi}}_{\rm s}$ and $\hat{\boldsymbol{\xi}}_{\rm f}$, respectively.

To separate the slow and fast magnetic modes, we assume the linearized continuity equation ($\omega\rho_k = \rho_0 \boldsymbol{k}\cdot\boldsymbol{v}_k$) and the induction equation ($\omega\,\boldsymbol{b}_k = \boldsymbol{k}\times(\boldsymbol{B}_0\times\boldsymbol{v}_k)$) are statistically true. From these, we get the Fourier components of the density and non-Alfvénic magnetic field:

$$\begin{aligned}\rho_k &= (\rho_0\Delta v_{k,{\rm s}}/c_{\rm s})\hat{\boldsymbol{k}}\cdot\hat{\boldsymbol{\xi}}_{\rm s} + (\rho_0\Delta v_{k,{\rm f}}/c_{\rm f})\hat{\boldsymbol{k}}\cdot\hat{\boldsymbol{\xi}}_{\rm f}\\ &\equiv \rho_{k,{\rm s}} + \rho_{k,{\rm f}},\end{aligned} \tag{A35}$$

$$\begin{aligned}b_k &= (B_0\Delta v_{k,{\rm s}}/c_{\rm s})|\hat{\boldsymbol{B}}_0\times\hat{\boldsymbol{\xi}}_{\rm s}| + (B_0\Delta v_{k,{\rm f}}/c_{\rm f})|\hat{\boldsymbol{B}}_0\times\hat{\boldsymbol{\xi}}_{\rm f}|\\ &\equiv b_{k,{\rm s}} + b_{k,{\rm f}},\end{aligned} \tag{A36}$$

$$\begin{aligned}&= \rho_{k,{\rm s}}(B_0/\rho_0)(|\hat{\boldsymbol{B}}_0\times\hat{\boldsymbol{\xi}}_{\rm s}|/\hat{\boldsymbol{k}}\cdot\hat{\boldsymbol{\xi}}_{\rm s})\\ &\quad + \rho_{k,{\rm f}}(B_0/\rho_0)(|\hat{\boldsymbol{B}}_0\times\hat{\boldsymbol{\xi}}_{\rm f}|/\hat{\boldsymbol{k}}\cdot\hat{\boldsymbol{\xi}}_{\rm f}),\end{aligned} \tag{A37}$$

where $\Delta v_k \propto v_k^+ - v_k^-$ (the superscripts '+' and '−' represent opposite directions of wave propagation) and the subscripts 's' and 'f' stand for 'slow' and 'fast' modes, respectively. From equations (A35), (A36) and (A37), we can obtain $\rho_{k,{\rm s}}$, $\rho_{k,{\rm f}}$, $b_{k,{\rm s}}$, and $b_{k,{\rm f}}$ in Fourier space.

APPENDIX B: SCALE-DEPENDENT ANISOTROPY

Fig. B1(a) shows the shapes of Alfvén eddies of different sizes. The left three panels show an increased anisotropy as we move from the top (large eddies) to the bottom (small eddies). The horizontal axes of the left panels are parallel to $\boldsymbol{B}_0$. Structures in the perpendicular plane (right panels) do not show a systematic elongation. However, Fig. B1(b) shows that the velocity of the fast modes exhibits isotropy. Data are from a simulation with 216^3 grid points, $M_{\rm s} = 2.3$, and $\beta = 0.2$.

This paper has been typeset from a TEX/LATEX file prepared by the author.